JACS
JOURNAL OF THE AMERICAN CHEMICAL SOCIETY

ARTICLE

pubs.acs.org/JACS

Control of the Mutual Arrangement of Cyclometalated Ligands in Cationic Iridium(III) Complexes. Synthesis, Spectroscopy, and Electroluminescence of the Different Isomers

Jesús M. Fernández-Hernández,*[,†,§] Cheng-Han Yang,[†,§] Juan I. Beltrán,[⊥,∥] Vincent Lemaur,[⊥] Federico Polo,[†,§] Roland Fröhlich,[‡] Jêrôme Cornil,[⊥] and Luisa De Cola*[,†,§]

[†]Physikalisches Institut, Mendelstrasse 7, and [‡]Organisch-Chemisches Institut, Corrensstrasse 40, Westfälische Wilhelms-Universität Münster, 48149 Münster, Germany

[§]Center for Nanotechnology (CeNTech), Heisenbergstrasse 11, 48149 Münster, Germany

[⊥]Service de Chimie des Matériaux Nouveaux, Université de Mons, Place du Parc 20, 7000 Mons, Belgium

[∥]Departamento de Física Teórica de la Materia Condensada, Universidad Autónoma de Madrid, 28049 Madrid, Spain

Supporting Information

ABSTRACT: Synthetic control of the mutual arrangement of the cyclometalated ligands (C^N) in Ir(III) dimers, $[Ir(C^N)_2Cl]_2$, and cationic bis-cyclometalated Ir(III) complexes, $[Ir(C^N)_2(L^L)]^+$ (L^L = neutral ligand), is described for the first time. Using 1-benzyl-4-(2,4-difluorophenyl)-1*H*-1,2,3-triazole (HdfptrBz) as a cyclometalating ligand, two different Ir(III) dimers, $[Ir(dfptrBz)_2Cl]_2$, are synthesized depending on the reaction conditions. At 80 °C, the dimer with an unusual mutual *cis*-C,C and *cis*-N,N configuration of the C^N ligands is isolated. In contrast, at higher temperature (140 °C), the geometrical isomer with the common *cis*-C,C and *trans*-N,N arrangement of the C^N ligand is obtained. In both cases, an asymmetric bridge, formed by a chloro ligand and two adjacent nitrogens of the triazole ring of one of the cyclometalated ligands, is observed. The dimers are cleaved in coordinating solvents to give the solvento complexes $[Ir(dfptrBz)_2Cl(S)]$ (S = DMSO or acetonitrile), which maintain the C^N arrangement of the parent dimers. Controlling the C^N ligand arrangement in the dimers allows for the preparation of the first example of geometrical isomers of a cationic bis-cyclometalated Ir(III) complex. Thus, *N,N-trans*-$[Ir(dfptrBz)_2(dmbpy)]^+$ (dmbpy = 4,4′-dimethyl-2,2′-bipyridine), with *cis*-C,C and *trans*-N,N arrangement of the C^N ligands, as well as *N,N-cis*-$[Ir(dfptrBz)_2(dmbpy)]^+$, with *cis*-C,C and *cis*-N,N C^N ligand orientation, are synthesized and characterized. Interestingly, both isomers show significantly different photophysical and electroluminescent properties, depending on the mutual arrangement of the C^N ligands. Furthermore, quantum chemical calculations give insight into the observed photophysical experimental data.

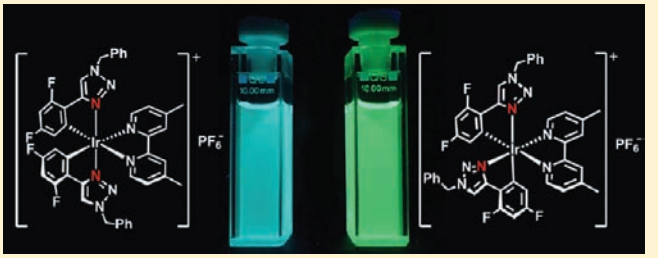

INTRODUCTION

Phosphorescent Ir(III) complexes have been used in various applications such as biological labeling reagents,[1] photosensitizers for light-driven catalytic water reduction,[2] single oxygen sensitizers,[3] and sensors.[4] In particular, the most important application of the Ir(III) complexes is as emitters in electroluminescent devices including organic light-emitting devices (OLEDs)[5−7] and light-emitting electrochemical cells (LEECs).[8−11] This is due to their luminescent excited states that are triplet in nature, relatively short excited-state lifetimes, high photoluminescence quantum yields, and facile color tuning through ligand-structure control. The triplet nature of the emission, due to the strong spin−orbit coupling in these complexes, is of great importance. In fact, in electroluminescent devices the luminescence from a triplet state allows the harvesting of both the singlet and triplet excitons, produced when electrons and holes recombine, reaching up to 100% internal efficiency. Most of the Ir(III) complexes used in OLEDs are based on tris-cyclometalated Ir(III), $[Ir(C^N)_3]$, or neutral heteroleptic bis-cyclometalated $[Ir(C^N)_2(L^X)]$ complexes (C^N = C-, N-donor cyclometalating ligand, L^X = ancillary ligand).[7,12] These complexes are generally synthesized through a two-step process, the first step being a reaction between the HC^N ligand and $IrCl_3 \cdot nH_2O$ to form a dichloro-bridged dinuclear Ir(III) dimer, $[Ir(C^N)_2(\mu\text{-}Cl)]_2$.[7,13] This precursor has been employed to make a great number of complexes due to the diversity of ligands which can be used for the preparation of the dimer. In almost all cases, the dimers that are fully characterized in the literature show a mutual *trans*-N,N arrangement of the N-coordinated

Received: February 23, 2011
Published: May 20, 2011

heterocyclic rings.[7,14,15] Further reaction of the dichloro-bridged dimer with a third cyclometalating ligand yields tris-cyclometalated complexes that can be homoleptic, $[Ir(C^N)_3]$, if the C^N are identical or heteroleptic, $[Ir(C^N)_2(C'^N')]$, if a different C′^N′ is used. For these tris-cyclometalated Ir(III) complexes two isomers are possible, facial (*fac*) and meridional (*mer*).[16−18] The *mer* isomer can be thermally or photochemically isomerized to the more stable *fac* isomer.[16−18] Both isomers present markedly different photophysical properties that are of great importance for their different applications (e.g., OLEDs).[18,19] The chloride dimer can also react with chelating ligands, leading to a wide range of neutral bis-cyclometalated complexes $[Ir(C^N)_2(L^X)]$ (L^X = anionic ligands as β-diketonates, picolinates, pyridineazolates, etc.) or charged complexes $[Ir(C^N)_2(L^L')]^+$ (e.g. L^L′ = neutral ligands such as diimines, phosphines, etc.).[11,12,15,20,21] Generally, for neutral bis-cyclometalated complexes, the *cis*-C,C or *trans*-N,N arrangement of the C^N ligand is maintained as in the parent dimer. Recently, Nazeeruddin et al. observed the isomerization of a neutral bis-cyclometalated Ir(III) complex from a *trans*-N,N to a *cis*-N,N disposition of the C^N ligands upon sublimation, and they described the different behavior of the two isomers in OLEDs.[22] Simultaneously, Chi et al. described a similar isomerization during the synthesis of neutral bis-cyclometalated iridium complexes at high temperature, and different properties for the two isomers were observed.[23] However, to the best of our knowledge, similar isomerization in cationic bis-cyclometalated Ir(III) complexes has not been observed yet, and all cationic complexes $[Ir(C^N)_2(L^L')]^+$ described in the literature have a *trans*-N,N disposition of the heterocycle ring of the C^N ligand.

One of the advantages of cyclometalated Ir(III) complexes is that the emission color can be tuned by judicious design of the chemical structure and nature of the cyclometalated ligands.[7,21,24] Although Ir(III) complexes that emit from blue to near-infrared have been reported, the amount of highly efficient blue phosphorescent Ir(III) compounds is still limited. 2-Phenylpyridine (ppy) and its derivatives are typical compounds used as C^N ligands. One approach to obtain blue-emitting complexes is to stabilize the highest occupied molecular orbital (HOMO) on the arylpyridine moieties by placing electron-withdrawing substituents on the aryl group; however, a more effective strategy is to raise the lowest unoccupied molecular orbital (LUMO) of the complex by replacing the pyridine moiety with other N-heterocyclic groups, e.g., azole[18,25,26] or *N*-heterocyclic carbene,[26,27] that have significantly higher reductions potentials (LUMO) than that of pyridine. More versatile ligands are 1,2,3- or 1,2,4-triazole derivatives. In our group, we have successfully used pyridyl-1,2,3-[8,28,29] and -1,2,4-triazoles[6,30] as ancillary ligands to modify the emission of the Ir(III) complexes. Furthermore, the 1,4-disubstituted-1*H*-1,2,3-triazoles can be easily prepared using "click chemistry", which is known to be a very reliable synthetic tool in terms of high yields, selectivity, and versatility.[31] On the other hand, 1-substituted-4-aryl-1*H*-1,2,3-triazole can also act as a cyclometalating ligand in Ir(III) complexes, but only a few examples have been recently reported.[29,32,33]

Herein, we present our results toward the synthesis of highly emitting charged Ir(III) complexes containing 1,4-disubstituted-1*H*-1,2,3-triazoles as cyclometalating ligands. We have synthesized a series of Ir(III) dimers, $[Ir(C^N)_2Cl]_2$ (C^N = 1-benzyl-4-(2,4-difluorophenyl)-1*H*-1,2,3-triazolyl, dfptrBz), that show an unusual coordination of the Ir center. Interestingly, depending on the reaction conditions, we can control the mutual arrangement of the cyclometalated ligands around the Ir atom. Thus, performing the reaction at high temperature (140 °C), we have isolated the Ir(III) dimer, which shows a *cis*-C,C and *trans*-N,N disposition of the chelating ligands, as is usually observed for dichloro-bridged cyclometalated Ir(III) dimers. However, at a lower temperature (80 °C), we have obtained and fully characterized an isomer that shows a unique mutual *cis*-C,C and *cis*-N,N arrangement of the cyclometalated ligands. In both cases, instead of the usual symmetric μ-dichloro bridge described for cyclometalated Ir(III) dimers, an asymmetric bridge formed by a chloro ligand and two adjacent nitrogens of the triazole ring of one of the cyclometalated ligands is obtained. These new dimers have been used as precursors to prepare cationic bis-cyclometalated complexes $[Ir(C^N)_2(L^L)]^+$ (C^N = dfptrBz, L^L = diimine), which show different photophysical properties depending on the mutual disposition of the C^N ligands. The experimental spectroscopic data have been further rationalized by means of quantum chemical calculations. We have also studied the behavior of the two different isomers in electroluminescent devices, both polymer light-emitting diodes (PLEDs) and LEECs. The findings clearly show how important it is to control and isolate different isomers which can be formed during the synthesis of heteroleptic complexes.

EXPERIMENTAL SECTION

General Information and Materials. The solvents were dried using standard distillation procedures. All other reagents were used as received from commercial sources, unless otherwise stated. 1-Benzyl-4-(2,4-difluorophenyl)-1*H*-1,2,3-triazole (HdfptrBz) was prepared as recently reported.[33] NMR spectra were recorded on an ARX 300 or AMX 500 instrument from Bruker Analytische Messtechnik (Karlsruhe, Germany). The ^{1}H NMR chemical shifts (δ) of the signals are given in ppm and referenced to residual protons in the deuterated solvents: $CDCl_3$ (7.26 ppm), CD_2Cl_2 (5.32 ppm), DMSO-d_6 (2.50 ppm), or CD_3CN (1.94 ppm). The ^{19}F NMR chemical shifts are referenced to $CFCl_3$ (0.00 ppm) as an internal standard. For the dimer complexes, ^{1}H,^{1}H gCOSY and ^{19}F,^{19}F gCOSY were measured. The signal splittings are abbreviated as follows: s = singlet; d = doublet; dd = doublet of doublet; t = triplet; q = quartet; m = multiplet. All coupling constants (*J*) are given in hertz (Hz). Mass spectrometry was performed in the Department of Chemistry, University of Münster. Electrospray ionization (ESI) mass spectra were recorded on a Bruker Daltonics (Bremen, Germany) MicroTof instrument with loop injection. Elemental analysis was recorded at the University of Milan, Italy.

High-Performance Liquid Chromatography (HPLC). HPLC was carried out on a JASCO apparatus equipped with LC-Net II/ADC controller, two pumps PU-2087, degasser DG-2080-53, and UV/vis detector UV-2075. Columns were purchased from Mz Analysentechnik GmbH. The ratio of **N,N-cis-3** and **N,N-trans-3** was determined by analytical HPLC. A MeOH solution (20 μL) was injected into a KromaSil 100 C18 5 μm column (250 × 3 mm), operating at 30 °C. The detection wavelength was fixed at 254 nm. A mobile phase of H_2O (0.05% formic acid)/methanol (0.025% formic acid), with a gradient 70:30 to 0:100 in 40 min and 0:100 to 70:30 in 10 min, and a flow rate of 0.8 mL/min were used. Under these conditions, **N,N-cis-3** has a retention time of 29 min and **N,N-trans-3** of 30 min. The compounds were purified on a milligram scale by means of semipreparative HPLC using a KromaSil 100 C8 7 μm column (250 × 30 mm), operating at 30 °C. A solution of 10 mg of the mixture in 2 mL of MeOH was injected. The detection wavelength was fixed at 254 nm. A mobile phase of H_2O (0.05% formic acid)/methanol (0.025% formic acid), with a gradient

50:50 to 0:100 in 40 min and 0:100 to 50:50 in 3 min, and a flow rate of 20 mL/min were used.

Preparation. *trans-[(dfptrBz)$_4$Ir$_2$Cl$_2$]* (***N,N-trans-dimer***). The ligand HdfptrBz, prepared according to our just-published procedure[33] (1.0 g, 3.69 mmol), $IrCl_3 \cdot H_2O$ (0.59 g, 1.68 mmol), and 16 mL of 2-ethoxyethanol/water (3:1) were heated at 140 °C for 20 h under a nitrogen atmosphere and protected from light using aluminum foil. After the reaction cooled to room temperature, 5 mL of water was added. The resulting pale yellow solid was isolated by filtration and washed successively with water (10 mL) and Et_2O (60 mL). The product was suspended in CH_2Cl_2 (10 mL), and the addition of Et_2O (100 mL) yielded a pale yellow solid that was filtered and air-dried. Yield: 0.86 g (66%). ^{1}H NMR (CD_2Cl_2, 500 MHz) δ: major set, 8.00 (d, J = 1.3, 1H), 7.71 (d, J = 1.5, 1H), 7.64−7.56 (m, 3H), 7.54−7.34 (m, 14H), 7.24 (d, J = 1.5, 1H), 7.22−7.12 (m, 2H), 6.56−6.50 (m, 2H), 6.50−6.24 (m, 4H), 5.78 (AB, J = 14.8, 1H), 5.78 (AB, J = 14.6, 1H), 5.76−5.71 (m, 2 H), 5.74 (AB, J = 14.6, 1H), 5.62 (AB, J = 14.8, 1H), 5.66 (dd, J = 9.5, 2.3, 1H), 5.51 (AB, J = 14.7, 1H), 5.45 (AB, J = 17, 1H), 5.41 (AB, J = 17, 1H), 5.37 (AB, J = 14.7, 1H), 5.09 (dd, J = 9.1, 2.3 Hz, 1H). ^{19}F{^{1}H} NMR (CD_2Cl_2, 282 MHz) δ: major set, −108.91 (d, J = 7.7), −109.00 (d, J = 7.8), −110.72 (d, J = 7.8), −110.88 (d, J = 7.0), −112.52 (d, J = 6.6), −112.75 (d, J = 7.0), −112.86 (d, J = 7.7), −113.01 (d, J = 6.6); minor set, −109.16 (d, J = 7.7), −109.56 (d, J = 7.7), −109.71 (d, J = 7.4), −110.65 (d, J = 7.8), −110.81 (d, J = 7.2), −111.51 (d, J = 6.7,), 112.71 (d, J = 7.4), −113.22 (d, J = 7.5), −113.24 (d, J = 7.2) −113.52 (d, J = 6.8). m/z (ESI-MS+): 1559.18 $[M+Na]^+$, 1501.23 $[M-Cl]^+$. Anal. Calcd for $C_{60}H_{40}Cl_2F_8Ir_2N_{12}$: C, 46.91; H, 2.62; N, 10.94. Found: C, 46.54; H, 2.73; N, 10.60.

cis-[(dfptrBz)$_4$Ir$_2$Cl$_2$] (***N,N-cis-dimer***). A mixture of HdfptrBz (0.54 g, 1.99 mmol), $IrCl_3 \cdot H_2O$ (0.22 g, 0.62 mmol), and 8 mL of 2-ethoxyethanol/water (3:1) was heated at 80 °C for 20 h, protected from light. The reaction was cooled to room temperature and 5 mL of water added. The resulting pale yellow solid was filtered off and washed successively with water (10 mL) and Et_2O (60 mL). The solid was purified by chromatography on silica gel using cyclohexane/EtOAc (2:1 to 1:1) mixture as eluent. Yield: 0.29 g (60%). ^{1}H NMR (CD_2Cl_2, 500 MHz) δ: major set, 7.79 (d, J = 1.9, 1H), 7.75−7.71 (m, 2H), 7.58−7.26 (m, 12H), 7.24−7.18 (m, 2H), 7.16 (t, J = 7.8, 2H), 7.07−7.02 (m, 2H), 7.00−6.94 (m, 2H), 6.87 (dd, J = 10.1, 2.3, 1H), 6.67 (d, J = 7.2, 2H), 6.64−6.58 (m, 1H), 6.57−6.49 (m, 1H), 6.28 (m, 2H), 5.91 (dd, J = 9.3, 2.3, 1H), 5.80 (AB, J = 14.8, 1H), 5.72 (AB, J = 14.8, 1H), 5.48 (dd, J = 9.5, 2.5, 1H), 5.37 (s, 2H), 5.25 (AB, J = 14.7, 1H), 5.14 (AB, J = 14.7, 1H), 5.12 (AB, J = 15.6, 1H), 4.68 (AB, J = 15.6, 1H). ^{19}F{^{1}H} NMR (CD_2Cl_2, 282 MHz) δ: major set, −109.40 (d, J = 7.3), −110.08 (d, J = 7.3 Hz), −110.88 (d, J = 7.0), −111.54 (d, J = 6.9), −112.88 (d, J = 7.3), −113.15 (d, J = 6.9), −114.36 (d, J = 7.3), −114.70 (d, J = 7.0); minor set, −109.83 (d, J = 6.6), −110.15 (d, J = 6.9), −111.40 (d, J = 6.5 Hz), −111.88 (d, J = 6.9), −112.21 (d, J = 6.8), −112.39 (d, J = 6.9), −113.71 (d, J = 6.9), −114.05 (d, J = 6.5), −114.07 (d, J = 6.8), −114.39 (d, J = 7.0), −114.57 (d, J = 6.8), −114.79 (d, J = 7.2), −113.71 (d, J = 6.9), −114.05 (d, J = 6.5). m/z (ESI-MS+): 1559.18 $[M+Na]^+$, 1501.23 $[M-Cl]^+$. Anal. Calcd for $C_{60}H_{40}Cl_2F_8Ir_2N_{12}$: C, 46.91; H, 2.62; N, 10.94. Found: C, 47.35, H, 2.78; N, 10.72.

Preparation of Solvento Complexes. Ten milligrams of the corresponding dimer was dissolved in DMSO-d_6 or CD_3CN (0.7 mL):

N,N-cis-[Ir(dfptrBz)$_2$(DMSO-d$_6$)Cl] (***N,N-cis-2a***). ^{1}H NMR (DMSO-d_6, 300 MHz) δ: 8.72 (s, 1H), 8.49 (s, 1H), 7.55 (d, J = 7.4, 1H), 7.50−7.15 (m, 7H), 7.09 (t, J = 8.5, 1H), 7.00 (m, 2H), 6.74 (t, J = 8.8, 1H), 5.91 (s, 2H), 5.78 (d, J = 7.1, 1H), 5.51 (AB, J = 17.1, 2H). ^{19}F{^{1}H} NMR (DMSO-d_6, 282 MHz) δ: −109.25 (d, J = 6.9, 1F), −111.11 (d, J = 6.3, 1F), −112.06 (d, J = 6.9, 1F), −112.40 (d, J = 6.3, 1F).

N,N-trans-[Ir(dfptrBz)$_2$(DMSO-d$_6$)Cl] (***N,N-trans-2a***). ^{1}H NMR (DMSO-d_6, 300 MHz) δ: 8.83 (s, 1H), 8.81 (s, 1H,), 7.61−7.24 (m, 10H), 6.88−6.66 (m, 2H), 5.91 (s, 2H), 5.89 (s, 2H), 5.51−5.31 (m, 2H). ^{19}F{^{1}H} NMR (282 MHz, DMSO-d_6) δ: −109.96 (d, J = 7.0, 1F), −110.46 (d, J = 6.6, 1F), −111.66 (d, J = 7.0, 1F), −112.38 (d, J = 6.6, 1F).

N,N-cis-[Ir(dfptrBz)$_2$(CD$_3$CN)Cl] (***N,N-cis-2b***). Slow evaporation gave colorless crystals suitable for X-ray crystallography. ^{1}H NMR (CD_3CN, 300 MHz) δ: 8.18 (d, J = 2.1, 1H), 7.92 (d, J = 1.5, 1H), 7.71 (dd, J = 9.9, 2.4, 1H), 7.55−7.37 (m, 6H), 7.35−7.23 (m, 2H), 7.13−6.99 (m, 2H), 6.74 (ddd, J = 10.4, 9.5, 2.4, 1H,), 6.37 (ddd, J = 10.5, 9.5, 2.4, 1H), 5.74 (dd, J = 9.8, 2.4, 1 H), 5.80 (AB, J = 15.1, 1H), 5.75 (AB, J = 15.1, 1H) 5.35 (AB, J = 15.4, 2H). ^{19}F{^{1}H} NMR (CD_3CN, 282 MHz) δ: −111.80 (d, J = 6.8, 1H), −113.68 (d, J = 6.7, 1H), −114.63 (d, J = 6.8, 1H), −114.83 (d, J = 6.7, 1H).

N,N-trans-[Ir(dfptrBz)$_2$(CD$_3$CN)Cl] (***N,N-trans-2b***). Slow evaporation gave colorless crystals suitable for X-ray crystallography. ^{1}H NMR (CD_3CN, 300 MHz) δ: 8.20 (s, 1H), 8.18 (s, 1H), 7.61−7.34 (m, 10H), 6.54−6.30 (m, 4H), 5.81 (s, 2H), 5.79 (AB, J = 15.2, 1H), 5.76 (AB, J = 15.2, 1H), 5.56 (dd, J = 9.1, 2.2, 1H), 5.44 (dd, J = 9.7, 2.1, 1H). ^{19}F{^{1}H} NMR (CD_3CN, 282 MHz) δ: −112.33 (d, J = 7.0, 1F), −112.75 (d, J = 6.9, 1F), −113.77 (d, J = 7.0, 1F), −114.46 (d, J = 7.0, 1F).

N,N-trans-[Ir(dfptrBz)$_2$(dmbpy)]PF$_6$ (***N,N-trans-3***). Method A: 188 mg (0.122 mmol) of **N,N-trans-dimer** and 47 mg (0.257 mmol) of 4,4′-dimethyl-bipyridine (dmbpy) were suspended in 2-ethoxyethanol (7 mL). The reaction mixture was flushed with nitrogen for 20 min and refluxed for 17 h, protected from light. After the mixture cooled, water (15 mL) was added. The mixture was extracted with Et_2O (2 × 20 mL). The aqueous phase was heated at 80 °C to remove traces of Et_2O. Addition of an aqueous solution of NH_4PF_6 (1 g in 10 mL of water) yielded a yellow precipitated that was filtered and washed with water (20 mL) and Et_2O (20 mL). The solid was recrystallized in MeCN/Et_2O. Yield: 180 mg (70%).

Method B: 188 mg (0.122 mmol) of **N,N-trans-dimer** and 47 mg (0.257 mmol) of dmbpy were suspended in 2-ethoxyethanol (7 mL). The reaction mixture was flushed with nitrogen for 20 min and refluxed for 17 h. After cooling, the solution was evaporated to dryness. Chromatography column was performed using dichloromethane/MeOH (15:1) as eluent to obtain the chloride derivate. This complex was dissolved in the smallest amount of MeOH. Slow addition of a saturated solution of NH_4PF_6 in MeOH rendered a bright yellow suspension. The mixture was stirred for 30 min. The resulting solid was filtered off and washed with water, MeOH, and diethyl ether. Yield: 160 mg (62%). ^{1}H NMR ($CDCl_3$, 300 MHz) δ: 8.50 (s, 2H), 7.83 (d, J = 5.6, 2H), 7.65 (d, J = 1.3, 2H), 7.48−7.35 (m, 6H), 7.27−7.18 (m, 4H), 7.16 (dd, J = 5.6, 0.9, 1H), 6.55−6.41 (m, 1H), 5.64 (dd, J = 8.7, 2.2, 1H), 5.49 (AB, J = 15, 2H), 5.38 (AB, J = 15, 2H), 2.62 (s, 6H). ^{19}F{^{1}H} NMR ($CDCl_3$, 282 MHz) δ: −72.89 (d, J = 712.7, 6F, PF_6), −108.42 (d, J = 7.8, 2F), −111.13 (d, J = 7.8, 2F). m/z (ESI-MS+): 917.23 $[M-PF_6]^+$. Anal. Calcd for $C_{42}H_{32}F_{10}IrN_8P$: C, 47.50; H, 3.04; N, 10.55. Found: C, 47.31; H, 3.05; N, 10.50.

N,N-trans-[Ir(dfptrBz)$_2$(dmbpy)]BF$_4$ (***N,N-trans-3′***). Following method B as for **N,N-trans-3**, a suspension of $NaBF_4$ in MeOH was slowly added to a MeOH solution of the chloride derivate. The reaction mixture was vigorously stirred overnight at room temperature and protected from light. The mixture was concentrated to dryness and washed with water (20 mL). The yellow solid was filtered off and washed with water (50 mL) and diethyl ether (50 mL), successively. The resulting solid was dried under vacuum and recrystallized in MeCN/Et_2O. Yield: 178 mg (73%). ^{1}H NMR ($CDCl_3$, 300 MHz) δ: 8.70 (s, 2H), 7.82 (d, J = 5.6, 2H), 7.66 (d, J = 1.3, 2H), 7.49−7.33 (m, 6H, Ph), 7.25−7.22 (m, 4H, Ph), 7.15 (d, J = 5.6, 2H), 6.58−6.36 (m, 2H), 5.65 (dd, J = 8.7, 2.2, 2H), 5.50 (AB, J = 15, 2H), 5.39 (AB, J = 15, 2H), 2.65 (s, 6H). ^{19}F{^{1}H} NMR (282 MHz, $CDCl_3$) δ: −108.43 (d, J = 7.8, 2F), −111.14 (d, J = 7.8, 2F), −152.53 (b, $^{10}BF_4$), −152.56 to −152.60 (m, $^{10}BF_4$). m/z (ESI-MS+): 917.23 $[M-BF_4]^+$. Anal.

Calcd for $C_{42}H_{32}BF_8IrN_8$: C, 50.26; H, 3.21; N, 11.16. Found: C, 50.26; H, 3.39; N, 11.26.

*N,N-cis-[Ir(dfptrBz)$_2$(dmbpy)]PF$_6$ (**N,N-cis-3**).* To a solution of **N,N-cis-dimer** (105 mg, 0.068 mmol) in 2-ethoxyethanol (6 mL) was added dmbpy (27 mg, 0.143 mmol). The reaction mixture was placed under nitrogen atmosphere and heated to 80 °C for 20 h, protected from light. The resulting solution was concentrated to dryness under reduced atmosphere. Chromatography on silica gel was performed using dichloromethane/MeOH (15:1) as eluents. A mixture of cis:trans (1:0.7) chloride derivative isomers was obtained as a yellow solid. The mixture of isomers was separated by semipreparative HPLC. The different fractions were evaporated to remove all the MeOH and part of the water. By addition of NH_4PF_6 in water (1 gr in 10 mL water), a yellow precipitate was obtained. The solids were filtered and washed with water (4 × 5 mL), water:methanol (1:1; 5 mL), and Et_2O (5 mL) successively. Complex **N,N-cis-3** (50 mg, 35%) was obtained after drying under vacuum. ^{1}H NMR ($CDCl_3$, 400 MHz) δ: 8.31 (s, 1H), 8.28 (s, 1H), 7.92 (d, J = 5.9, 1H), 7.68 (d, J = 1.8, 1H), 7.65 (d, J = 5.6, 1H), 7.62 (d, J = 1.1, 1H), 7.39−7.32 (m, 6H), 7.30 (d, J = 6.5, 1H), 7.28−7.22 (m, 2H), 7.16 (m, 2H), 7.10 (d, J = 6.5, 1H), 6.53−6.39 (m, 2H), 6.08 (dd, J = 8.9, 2.3, 1H), 5.65 (dd, J = 8.7, 2.2, 1H), 5.53 (AB, J = 14.9, 1H), 5.51 (AB, J = 14.9, 1H), 5.44 (AB, J = 14.9, 1H), 5.40 (AB, J = 14.9, 1H), 2.61 (s, 3H), 2.47 (s, 3H). ^{19}F{^{1}H} NMR ($CDCl_3$, 282 MHz) δ: −72.89 (d, J = 712.7, 6F, PF_6), −108.46 (d, J = 7.8, 1F), −108.98 (d, J = 7.5, 1F), −110.92 (d, J = 7.8, 1F), −111.50 (d, J = 7.5, 1F). m/z (ESI-MS+): 917.23 $[M-PF_6]^+$. Anal. Calcd for $C_{42}H_{32}F_{10}IrN_8P$: C, 47.50; H, 3.04; N, 10.55. Found: C, 47.51; H, 3.10; N, 10.50.

Photophysical Measurement. Absorption spectra were measured on a Varian Cary 5000 double-beam UV−vis−NIR spectrometer and baseline corrected. Steady-state emission spectra were recorded on a HORIBA Jobin-Yvon IBH FL-322 Fluorolog 3 spectrometer equipped with a 450 W xenon-arc lamp, double-grating excitation and emission monochromators (2.1 nm/mm dispersion, 1200 grooves/mm), and a Hamamatsu R928 photomultiplier tube or a TBX-4-X single-photon-counting detector. Emission and excitation spectra were corrected for source intensity (lamp and grating) by standard correction curves. Time-resolved measurements were performed using the time-correlated single-photon-counting (TCSPC) option on the Fluorolog 3. NanoLED (402 nm; fwhm < 750 ps) with repetition rates between 10 kHz and 1 MHz was used to excite the sample. The excitation sources were mounted directly on the sample chamber at 90° to a double-grating emission monochromator (2.1 nm/mm dispersion; 1200 grooves/mm) and collected by a TBX-4-X single-photon-counting detector. The photons collected at the detector are correlated by a time-to-amplitude converter (TAC) to the excitation pulse. Signals were collected using an IBH Data Station Hub photon-counting module, and data analysis was performed using the commercially available DAS6 software (HORIBA Jobin Yvon IBH). The validity of the fit was assessed by minimizing the reduced χ^2 function and by visual inspection of the weighted residuals. Luminescence quantum yields were measured with a Hamamatsu Photonics absolute PL quantum yield measurement system (C9920-02) equipped with a L9799-01 CW xenon light source (150 W), monochromator, C7473 photonic multichannel analyzer, and integrating sphere and employing U6039-05 PLQY measurement software (Hamamatsu Photonics, Ltd., Shizuoka, Japan). All solvents were spectrometric grade. Deaerated samples were prepared by the freeze−pump−thaw technique. Low-temperature measurements were carried out in butyronitrile.

Photo and Thermal Isomerization. A mixture of **N,N-cis-3** and **N,N-trans-3** (1:0.7) in argon-purged MeCN was irradiated with UV light by using a Lot-Oriel 200 W high-pressure mercury lamp equipped with a 280−400 nm dichroic mirror (to remove IR and visible light), and after 47 h the proportion of the isomer was 1:0.08. However, when a solution of complex **N,N-trans-3** (10 mg) in ethyleneglycol (2 mL) was heated at 200 °C in pressure tube for 96 h and protected from light, no isomerization was observed.

X-ray Crystallography. Data sets were collected with a Nonius Kappa CCD diffractometer, equipped with a rotating anode generator. Programs used: data collection, COLLECT; data reduction, Denzo-SMN; absorption correction, SORTAV[35] and Denzo;[34] structure solution, SHELXS-97; structure refinement, SHELXL-97;[37] graphics, SCHAKAL.[38] Graphics show the thermal ellipsoids at the 50% probability level.

Electrochemistry. The electrochemical characterization (cyclic voltammetry and differential pulse voltammetry) of the metal complexes reported herein has been performed in acetonitrile/0.1 M tetrabutylammonium hexafluorophosphate (TBAH). The concentrations of the samples were 1 mM. Glassy carbon has been employed as working electrode, platinum wire as counter electrode, and platinum wire as quasi-reference electrode (QRE). Acetonitrile (Sigma-Aldrich, Chromasolv Plus, 99.9%) was used as received without any further purification. TBAH (electrochemical grade, ≥99%, Fluka) was used as supporting electrolyte, which was recrystallized from a 1:1 ethanol−water solution and dried at 60 °C under vacuum. For the electrochemical experiments, a CHI750C Electrochemical Workstation (CH Instruments, Inc., Austin, TX) was used. The electrochemical experiments were performed in a glass cell under an Ar atmosphere. To minimize the ohmic drop between the working and the reference electrodes, feedback correction was employed. The electrochemical experiments were performed by using a 1 mm diameter glassy carbon disk electrode (Cypress Systems). The working electrodes were stored in ethanol and before experiments were polished with a 0.05 μm diamond suspension (Metadi Supreme Diamond Suspension, Buehler) and ultrasonically rinsed with ethanol for 5 min. The electrode was electrochemically activated in the background solution by means of several voltammetric cycles at 0.5 V s^{-1} between the anodic and cathodic solvent/electrolyte discharges, until the same quality features were obtained. The reference electrode was a Pt QRE, which was separated from the catholyte by a glass frit (Vycor). The reference electrode was calibrated at the end of each experiment against the ferrocene/ferricenium couple, whose formal potential is 0.460 V against the KCl saturated calomel electrode (SCE); in the following, all potential values will be reported against SCE. A platinum ring or coil served as the counter electrode.

Computational Method. The ground-state geometry of the isomer complexes has been fully optimized in the absence of the counterion at the Density Functional Theory (DFT) level, starting from the X-ray structures. The chosen exchange correlation (XC) functional is the widely used B3LYP[39] in view of its good compromise between accuracy and computational cost; the basis set for the description of the electrons of nonmetallic atoms is 6-31G**,[40] while the LANL2DZ basis set has been used for iridium.[41] The characterization of the nature of the lowest-lying singlet and triplet excited states involved in absorption and emission properties, respectively, relies on time-dependent density functional theory (TD-DFT) calculations performed on the basis of the ground-state geometry, using the same functional and basis set. Our approach is motivated by previous works showing its adequacy to describe the electronic and optical properties of iridium complexes[9,42] and complexes with other metals.[43] Note that these calculations neglect intersystem crossing processes mixing states of the singlet and triplet manifold. All calculations were performed with the Gaussian03 package.

Device Fabrication. The solution-processed polymer light-emitting diode (PLED) devices were made using poly(9-vinylcarbazole) (PVK, M_w = 1 100 000; Aldrich). Poly(3,4-ethylenedioxythiophene): poly(styrenesulfonate) (PEDOT:PSS, 1:6 dispersion in water, electronic grade AI4083) and 1,3,5-tris[*N*-(phenyl)benzimidazole]benzene (TPBI) were purchased from HC Starck and Sensient Imaging Technologies, respectively. The device structure consists of a 120 nm transparent indium tin oxide (ITO) layer as the bottom electrode,

Scheme 1. Synthesis of N,N-trans- and N,N-cis-dimer and Complexes N,N-cis- and N,N-trans-2a,b

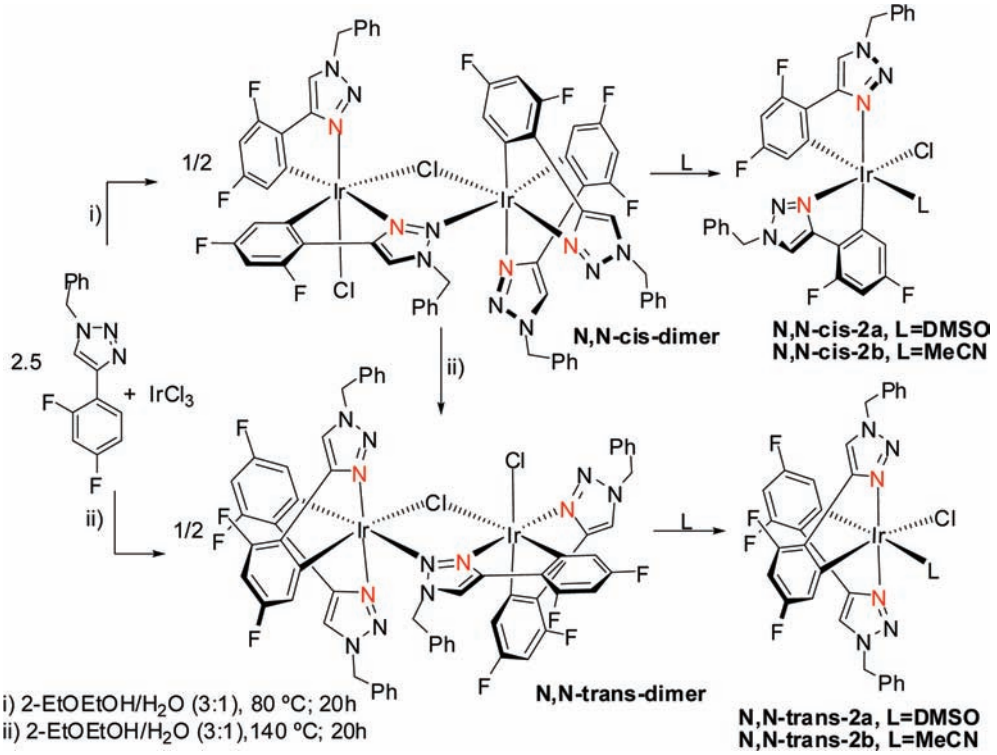

supported on a glass substrate. The ITO was treated for 10 min with UV/O_3 (UVO Cleaner 144AX, Jelight Co.) prior to any further processing. A 35−50 nm PEDOT:PSS layer was deposited from a water solution of the polymer on top of the ITO, using a P6700 spin-coater from Specialty Coating Systems. The device was then annealed at 180 °C for 2 min. The emissive layer was then spin-coated from a chlorobenzene solution containing 10.5 mg mL^{-1} of PVK, 30 wt % of 2,2′-(1,3-phenylene) bis[5-[4-(1,1-dimethylethyl)phenyl]]-1,3,4-oxadiazole (OXD-7) with respect to the PVK mass,and 7 wt % of Ir complex with respect to PVK:OXD-7 mass. The PVK:Ir complex in chlorobenzene solution was filtered through a 5 mm PTFE filter (Millex, Millipore) prior to spinning. To get a polymer layer with a thickness of 100 nm,the solution was spin-coated at 2000 rpm (40 s). An electron-transport layer was prepared via thermal evaporation of TPBI (30 nm) at a pressure of $(2.0-5.0) \times 10^{-6}$ mbar and a deposition rate of 2 Å s^{-1} using a MBraun evaporation chamber. The CsF electrode (1.5 nm) was evaporated on top of the TPBI film in a vacuum chamber at a pressure of $(2.0-5.0) \times 10^{-6}$ mbar and a rate of 1.5 Å s^{-1}. The aluminum top electrode (80 nm) was then immediately evaporated on top of the CsF (1.5 nm) without reducing the vacuum. All LEEC devices incorporating the iridium complexes were fabricated by spin-coating on ITO-covered glass substrates. The typical layer structure sketched in the schematic view of Figure 8b (below) consists of 100 nm of PEDOT:PSS and 70 nm of emitting layer composed of the chosen iridium complex. After deposition of the PEDOT:PSS layer, the emitting layer was prepared: 10 mg of iridium complexes in 1 mL of acetonitrile. The solution was filtered using a 0.1 mm PTFE filter and spin-coated on top of the PEDOT:PSS layer, and the resulting film was baked for 2 h at 80 °C inside a glovebox. Finally, a 100 nm thick aluminum layer was evaporated on top and used as a cathode. All measurements were run in an inert atmosphere directly after device fabrication. Voltage scans were then performed from zero to a preset positive voltage and then back to zero. The PLED and LEECs were characterized by attaching a computer-controlled low-noise single-channel direct-current (DC) power source that can act as both voltage source and current source, and a voltage meter or current meter (Keithley 2600, Keithley Instruments). Light from the diode was coupled to a photodiode and read out by an electrometer/high-resistance meter (Keithley 6517, Keithley Instruments). The output of the data was handled by a Labview (National Instruments)-based program. Calibration of the photodiode was done at a fixed current with a luminance meter (LS-100 Minolta). For every diode with a different spectral distribution of light, the photocurrent as measured by the photodiode was correlated to the light output in candles per square meter by this calibration. When recording an EL spectrum, a HORIBA Jobin-Yvon IBH FL-322 Fluorolog 3 spectrometer was used. The emission was corrected for the wavelength dependence of the spectrometer.

RESULTS AND DISCUSSION

Synthesis and NMR Characterization. The cyclometalating ligand 1-benzyl-4-(2,4-difluorophenyl)-1*H*-1,2,3-triazole (HdfptrBz) was synthesized by "click chemistry" by adapting a previously described procedure.[33,44] For the synthesis of the starting iridium dimers $[Ir(C^N)_2Cl]_2$ (C^N = dfptrBz), we followed the general description reported in the literature, which involves the reaction of $IrCl_3 \cdot nH_2O$ with cyclometalating ligand in a 3:1 mixture of 2-ethoxyethanol:water.[13] However, in our case, depending on the temperature, two different isomers of the dimer were obtained. When we carried out the reaction at low temperature (80 °C), we isolated complex **N,N-cis-dimer**, but at higher temperature (140 °C) the isomer **N,N-trans-dimer** was obtained (Scheme 1).

The elemental analysis and mass spectra of both complexes are in accordance with an iridium dimer of stoichiometry

dx.doi.org/10.1021/ja201691b |*J. Am. Chem. Soc.* 2011, 133, 10543–10558

Scheme 2. Synthesis of N,N-trans-3 and N,N-cis-3

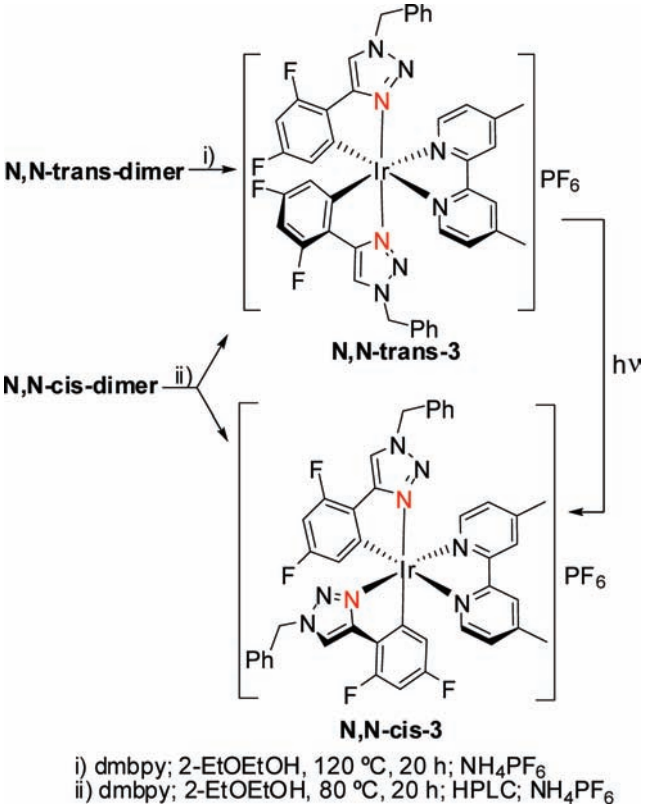

$[Ir(dfptrBz)_2Cl]_2$, but interestingly, their NMR spectra are different, pointing out the different arrangement of the cyclometalated ligands around the Ir atoms. The interpretation of the NMR spectra was, however, rather complex, and the assignments were done in accordance with the X-ray structure obtained for the **N,N-cis-dimer** (see X-ray Crystallography). Despite the purity of the complex, it is interesting to notice that the ^1H and $^{19}F\{^1H\}$ NMR spectra of **N,N-cis-dimer** in a noncoordinating solvent such as dichloromethane-d_2 show a major and minor set of signals (proportion 90:10, see Figures S1 and S2). The $^{19}F\{^1H\}$ spectrum shows eight doublets for the major set, corresponding to a complex with four nonequivalent cyclometalated dfptrBz ligands. This is indeed explained by the fact that the dimer is bridged in an asymmetric fashion (chloro ligand and a triazole moiety as bridging units), with the unique *cis*-C,C and *cis*-N,N disposition of the C^N ligand around iridium atom as observed in the X-ray structure. The minor set of signals in dichloromethane-d_2 could be due to the formation in solution of equilibria between different isomers depending on the bridging ligands (see Chart S1). To corroborate the special disposition of C^N ligand in **N,N-cis-dimer**, we dissolved the dimer in coordinated solvents such as DMSO-d_6 or CD_3CN in order to cleave the dimeric species into monomeric solvento complexes. The tendency of cyclometalated Ir(III) dimers, $[Ir(C^N)_2Cl]_2$, to form solvento complexes $[Ir(C^N)_2\,Cl(S)]$ (S = solvent) is well known in strongly coordinating solvents such as DMSO, CH_3CN, or DMF, keeping the same disposition of the cyclometalated ligand as in parent dimers.[45,46] The obtained *N,N-cis*-$[Ir(dfptrBz)_2Cl(DMSO)]$ (**N,N-cis-2a**) and *N,N-cis*-$[Ir(dfptrBz)_2Cl(CD_3CN)]$ (**N,N-cis-2b**) (Scheme 1) have simple NMR spectra

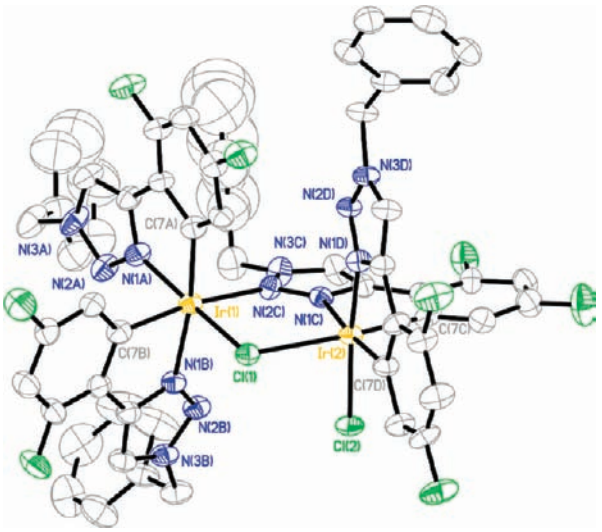

Figure 1. Crystal structure of **N,N-cis-dimer**. Hydrogen atoms have been removed for clarity. Selected bond lengths (Å) and angles (deg): Ir(1)−N(1A) 2.023(7); Ir(1)−C(7A), 2.045(10); Ir(1)−C(7B), 2.120(7); Ir(1)−N(1B), 2.120(7); Ir(1)−N(2C), 2.232(7); Ir(1)−Cl(1), 2.383(2); Ir(2)−N(1D), 2.021(7); Ir(2)−C(7C), 2.019(10); Ir(2)−C(7D), 2.028(9); Ir(2)−N(1C), 2.100(7); Ir(2)−Cl(2), 2.356(2); Ir(2)−Cl(1), 2.488(2); N(1A)−Ir(1)−N(1B), 95.8(3); C(7A)−Ir(1)−C(7B), 92.6(4); N(1A)−Ir(1)−N(2C), 95.9(3); N(2C)−Ir(1)−Cl(1), 89.6(2); N(1D)−Ir(2)−N(1C), 97.3(3); C(7C)−Ir(2)−C(7D), 95.0(4); Cl(2)−Ir(2)−Cl(1), 86.1(1); N(1C)−Ir(2)−Cl(1), 86.7(2).

(see Figures S3 and S4), and for each solvent only a single complex is observed. These results support that all species observed in dichloromethane-d_2 for **N,N-cis-dimer** have the same mutual *cis*-C,C and *cis*-N,N arrangement of the cyclometalated ligands around the metal and differ from the typical *cis*-C,C and *trans*-N,N geometry observed in the literature.[7,14,15] Furthermore, the structure of **N,N-cis-2b** has been resolved by X-ray crystallography and revealed the same disposition of the dfptrBz around the Ir as in the parent **N,N-cis-dimer** (see X-ray Crystallography).

As already mentioned, changing the reaction conditions leads to the formation of the **N,N-trans-dimer** (Scheme 1). The ^1H NMR spectrum of this species is also rather complex (see Figure S5). As for the cis dimer, this complex presents a major and a minor set of signals in the $^{19}F\{^1H\}$ NMR spectrum in dichloromethane-d_2, with the major set comprising eight signals shifted when compared to those of the **N,N-cis-dimer** (see Figure S6). These data suggest the presence of asymmetry in the bridging mode and the existence of different isomers (see Chart S2). To confirm our assignment, we made the corresponding solvento complexes by dissolving the **N,N-trans-dimer** in DMSO-d_6 or CD_3CN. The complexes *N,N-trans*-$[Ir(dfptrBz)_2Cl(DMSO)]$ (**N,N-trans-2a**) and *N,N-trans*-$[Ir(dfptrBz)_2Cl(CD_3CN)]$ (**N,N-trans-2b**) (Scheme 1) have similar NMR patterns, showing the presence of only one compound in each case (see Figures S3 and S4). We have isolated and analyzed the crystals of **N,N-trans-2b** (see X-ray Crystallography) that revealed a mutual *cis*-C,C and *trans*-N,N disposition of dfptrBz ligands in the complex, unlike the one observed in the **N,N-cis-2b** but similar to other solvento complexes derivatives from iridium dichloro-bridged dimers described in the literature.[45,46]

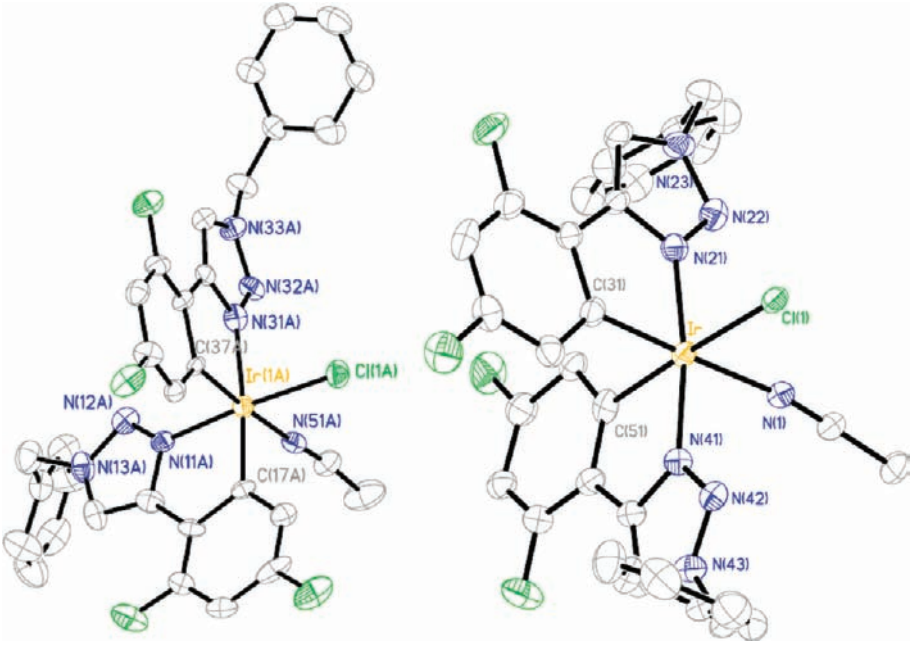

Figure 2. Crystal structure of **N,N-cis-2b** (left) and **N,N-trans-2b** (right) complexes. Hydrogen atoms have been removed for clarity. Selected bond lengths (Å) and angles (deg) of **N,N-cis-2b**: Ir(1A)−C(17A), 2.036(16); Ir(1A)−C(37A), 2.038(17); Ir(1A)−N(11A), 2.051(16); Ir(1A)−N(51A), 2.082(18); Ir(1A)−N(31A), 2.120(16); Ir(1A)−Cl(1A), 2.365(5); C(17A)−Ir(1A)−N(11A), 81.0(7); C(37A)−Ir(1A)−N(31A), 79.9(6); N(51A)−Ir(1A)−Cl(1A), 87.4(5). Selected bond lengths (Å) and angles (deg) of **N,N-trans-2b**: Ir−C(31), 2.007(14); Ir−N(41), 2.020(12); Ir−N(21), 2.029(12); Ir−C(51), 2.093(12); Ir−N(1), 2.103(12); Ir−C(l1), 2.464(3); C(31)−Ir−N(21), 79.5(6); N(41)−Ir−C(51), 79.0(4); N(1)−Ir−C(l1), 88.3(3); N(41)−Ir−N(21), 172.1(4); C(31)−Ir−N(1), 178.4(5); C(51)−Ir−C(l1), 175.9(3).

Indeed, the different symmetry of the cis and trans solvento complexes can be observed by comparison of their ^{1}H NMR spectra (Figure S3). For **N,N-trans-2b**, the proton signals of both cyclometalated ligands are overlapped due to their almost identical environment, while in **N,N-cis-2b** two set of signals (one for each ligand) are observed because the two ligands are in different environments.

Interestingly, **N,N-cis-dimer** isomerizes to **N,N-trans-dimer** when it is refluxed for 24 h in a 3:1 mixture of 2-ethoxyethanol: water (3:1). This suggests that **N,N-cis-dimer** is the kinetic isomer formed at lower temperature and can be transformed to the thermodynamically stable **N,N-trans-dimer** by thermal isomerization.

Complexes **N,N-trans-dimer** and **N,N-cis-dimer** can be used as precursors for the synthesis of new emitting Ir(III) complexes containing 1,4-disubstituted-1*H*-1,2,3-triazole as cyclometalating ligands. We studied their reactivity toward the symmetric diimine ligand, 4,4′-dimethyl-2,2′-bipyridine (dmbpy). Thus, complex *N,N-trans*-[Ir(dfptrBz)$_2$(dmbpy)]PF$_6$ (**N,N-trans-3**) was isolated in high yield through bridge-splitting reactions of the **N,N-trans-dimer** with dmbpy in 2-ethoxyethanol at 120 °C (17 h), followed by counterion exchange of the Cl^- with NH_4PF_6 (Scheme 2). The ^{1}H and ^{19}F{^{1}H} NMR spectra of **N,N-trans-3** (Figures S7 and S8) show one set of signals for the dfptrBz ligands according to a C_2-symmetry of the complex, confirming the *trans* disposition of the triazole rings. In order to obtain crystals of the complex, the BF_4 derivative *N,N-trans*-[Ir(dfptrBz)$_2$(dmbpy)]BF_4 (**N,N-trans-3′**) was isolated, and X-ray crystallography confirmed the disposition of the cyclometalated ligands (see X-ray Crystallography).

On the other hand, **N,N-cis-dimer** opens new possibilities to synthesize bis-cyclometalated Ir(III) complexes containing both N-heterocycle rings of the cyclometalated ligand in mutual *cis*-N,N disposition. The reaction **N,N-cis-dimer** with dmbpy at 80 °C (for 20 h) in 2-ethoxyethanol gave a mixture of isomeric complexes, *N,N-cis*-[Ir(dfptrBz)$_2$(dmbpy)]PF$_6$ (**N,N-cis-3**) and **N,N-trans-3** in a 1:0.7 proportion based on HPLC (see Scheme 2 and Figure S9). When the reaction was carried out at higher temperature (200 °C) in ethyleneglycol, the proportion was 1:0.25 (see Figure S10). Both isomers can be separated by reverse-phase HPLC. For complex **N,N-cis-3**, the ^{1}H and ^{19}F-{^{1}H} NMR spectra showed the existence of two set of signals for two different cyclometalated dfptrBz ligands according to the C_1-symmetry of the complex (see Figures S11 and S12). The structure was unequivocally assigned by X-ray crystallography analysis. Despite the great number of cationic bis-cyclometalated Ir(III) complexes described in the literature, to the best of our knowledge, **N,N-cis-3** is the first example of a fully characterized cationic bis-cyclometalated Ir(III) complex with mutual *cis*-C,C and *cis*-N,N arrangement of the cyclometalated ligands. Furthermore, complex **N,N-trans-3** can isomerize to give **N,N-cis-3** under UV irradiation, while thermal conversion cannot be accomplished (see Experimental Section). Thus, the irradiation of deareated MeCN solution containing the mixture **N,N-trans-3** and **N,N-cis-3** (0.7:1) yields after 47 h to an almost complete conversion of the trans into the cis isomer (0.08:1) (Figure S13). A proposed scheme to explain the different reactivity of the two dimers is illustrated in Chart S3 in the Supporting Information.

X-ray Crystallography. The structures of **N,N-cis-dimer**, **N,N-cis-2b**, **N,N-trans-2b**, **N,N-trans-3′**, and **N,N-cis-3** could be determined by the single-crystal X-ray crystallography.

The structure of **N,N-cis-dimer** shows the two Ir atoms in a distorted octahedral coordination (Figure 1). For each Ir, the dfptrBz acts as cyclometalated ligands in a mutual *cis*-C,C and

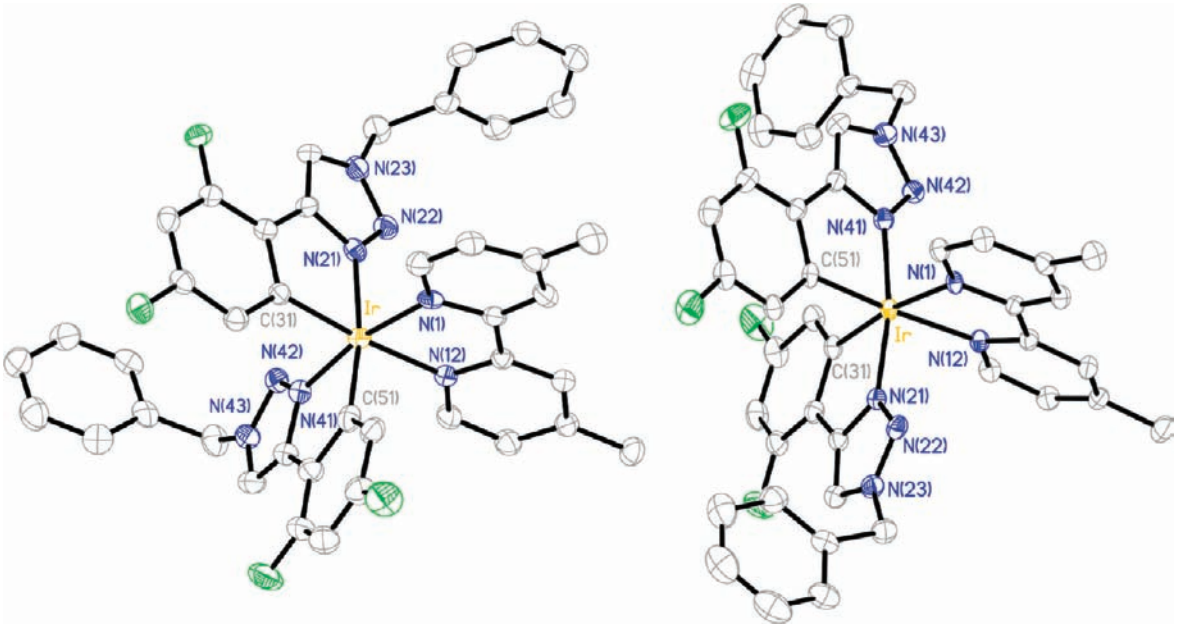

Figure 3. Crystal structure of **N,N-cis-3** (left) and **N,N-trans-3′** (right). Hydrogen atoms and counterion have been removed for clarity. Selected bond lengths (Å) and angles (deg) of **N,N-cis-3**: Ir−C(51), 2.003(9); Ir−N(41), 2.017(7); Ir−C(31), 2.038(7); Ir−N(1), 2.041(6); Ir−N(12), 2.104(6); Ir−N(21), 2.134(6); C(51)−Ir−N(41), 80.4(3); C(31)−Ir−N(21), 80.0(3); N(1)−Ir−N(12), 78.4(2); C(51)−Ir−N(21), 171.5(2); C(31)−Ir−N(12), 175.1(3); N(41)−Ir−N(1), 169.0(2). Selected bond lengths (Å) and angles (deg) of **N,N-trans-3′**: Ir−N(21), 2.015(4); Ir−C(31), 2.034(5); Ir−N(41), 2.032(4); Ir−N(1), 2.126(4); Ir−C(51), 2.033(5); Ir−N(12), 2.133(4); N(1)−Ir−N(12), 77.1(2); N(21)−Ir−C(31), 80.0(2); N(41)−Ir−C(51), 79.7(2); N(21)−Ir−C(51), 92.8(2); N(41)−Ir−N(1), 94.3(2), N(21)−Ir−N(41), 169.4(2); C(31)−Ir−N(1), 171.7(2); C(51)−Ir−N(12), 171.3(2); C(51)−Ir−C(31), 91.4(2).

cis-N,N configuration. The two Ir atoms (Ir1 and Ir2) are bridged by a Cl atom (Cl1) and by one triazole ring that coordinates to Ir1 by the N2C and to Ir2 by N1C, forming an asymmetric dimer. Different azoles (pyrazoles, imidazoles, 1,2,4-triazoles, 1,2,3-triazoles, etc.) are known to act as bridging ligands between two metal centers,[47] and some examples for Ir(III) complexes have been described.[48,49] The Ir2 atom completes its octahedral coordination binding to terminal Cl2. The bridging Cl has different distances (Ir1−Cl1 = 2.383(2) Å and Ir2−Cl1 = 2.488(2) Å) due to the larger trans influence of C- compared to N-donor ligands (comparing Ir1−C1 and Ir2−Cl1), while the terminal Cl has a shorter distance (Ir2−Cl2 = 2.356(2) Å). The two Ir−N distances trans to C-atoms (Ir2−N1*C* = 2.100(7) Å and Ir1−N1*B* = 2.120(7) Å) are significantly longer than the two Ir−N distances trans to Cl (Ir2−N1*D* = 2.021(7) Å and Ir1−N1*A* = 2.023(7) Å) due to the stronger trans influence of C compared to Cl. Furthermore, the distance Ir1−N2C (2.232(7) Å) corresponding to the bridging triazole is the longest among the Ir−N distances because it is trans to a C atom and has bridging character. There is a weak $\pi-\pi$ stacking between the benzyl groups of ligand A and ligand C (distance centroid (A)-centroid (C) = 4.064 Å). At the time of writing of this manuscript, this was the first crystal structure of an Ir(III) dimer $[Ir(C\hat{}N)_2Cl]_2$ (C^N = C-, N-donor cyclometalated ligand), with the C^N in a *cis*-C,C and *cis*-N,N arrangement. However, after submission of this manuscript, a paper by Bryce et al. described a similar configuration of the C^N ligand in an Ir(III) dimer.[49]

Complexes **N,N-cis-2b** and **N,N-trans-2b** show a distorted octahedral coordination (Figure 2). In **N,N-cis-2b** the C^N ligands are in the same *cis*-C,C and *cis*-N,N chelation geometry as observed in its parent **N,N-cis-dimer**. However, in **N,N-trans-2b** the triazole rings are mutually trans, giving a *cis*-C,C and *trans*-N,N chelation geometry. This arrangement of the ligands in **N,N-trans-2b** is the expected one for a solvento complex obtained from a **N,N-trans-dimer**.[46] A Cl atom and an acetonitrile molecule occupy the remaining coordination sites of the complexes. The Ir−Cl bond length is longer in **N,N-trans-2b** (Ir−Cl = 2.464(3) Å) than in **N,N-cis-2b** (Ir−Cl = 2.365(5)/2.359(9) Å) due to the higher trans influence of C-donor atoms compared to N-donor atoms.

In **N,N-trans-3′** the Ir(III) is in a distorted octahedral environment surrounded by two dfptrBz ligands bound in a *cis*-C,C and *trans*-N,N arrangement and dmbpy as a third ligand (Figure 3). This is the common disposition of the C^N ligands in the structure of cationic complexes, $[Ir(C\hat{}N)(L\hat{}L')]^+$ (L^L′ = neutral chelating ligand), described to date. Furthermore, the two Ir−$N_{triazole}$ distances (2.015(4) and 2.032(4) Å) are not significantly different and they are in the range of the Ir−$N_{pyrazole}$ distances observed in complexes $[Ir(C\hat{}N)_2(diimine)]^+$ (C^N = arylpyrazolyl ligands) described in the literature.[25,50] The Ir−C distances are similar (2.033(5) and 2.034(5) Å), while the Ir−N_{dmbpy} bond lengths (2.126(4) and 2.133(4) Å) are longer compared to Ir−$N_{triazole}$ of the complex and the Ir−N_{bpy} in $[Ir(bpy)_3]^{3+}$ [51] due to the strong trans influence of C-donor atoms of C^N ligand.

On the other hand, in **N,N-cis-3** the cyclometalating ligands have a *cis*-C,C and *cis*-N,N disposition around the Ir(III), as observed in the parent **N,N-cis-dimer** and in **N,N-cis-2b** complexes (Figure 3). As in **N,N-trans-3′**, the distorted octahedral coordination is completed by a chelating dmbpy ligand. The Ir−$N_{triazole}$ distances trans to C (2.134(6) Å) is significantly longer that the Ir−$N_{triazole}$ trans to N_{dmbpy} (2.017(7) Å) due to the larger trans influence of the C-donor atom. For similar

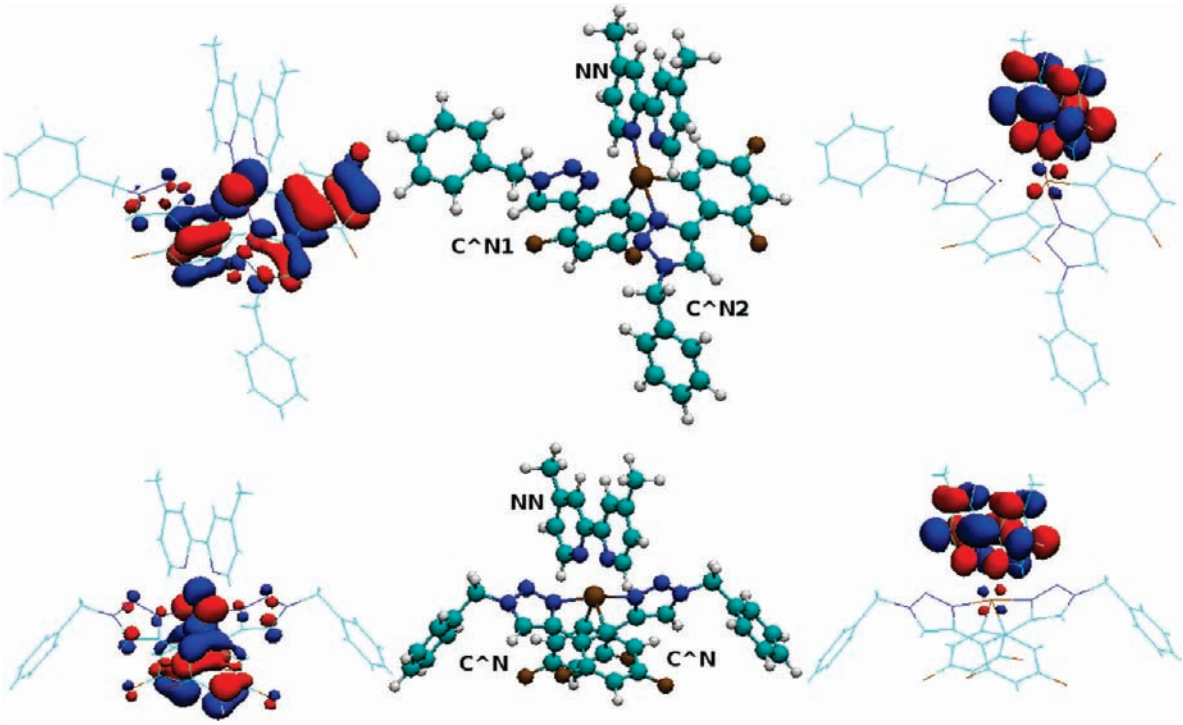

Figure 4. Electronic distribution for **N,N-cis-3** (top) and **N,N-trans-3** (bottom) of the HOMO (left) and LUMO (right) orbitals. In the center the calculated molecular structure is drawn for comparison.

Table 1. Energy and Localization of the Frontier Electronic Levels of N,N-cis-3 and N,N-trans-3

	N,N-cis-3					N,N-trans-3				
FO	*E*, eV	Ir	NN	C^N1	C^N2	*E*, eV	Ir	NN	C^N	C^N
HOMO-11	−9.65	6	89	1	3	−9.96	40	6	27	27
HOMO-10	−9.46	42	20	6	32	−9.54	2	97	1	1
HOMO-9	−9.45	39	7	31	24	−9.00	16	2	41	41
HOMO-8	−9.03	0	0	99	0	−9.00	4	1	48	48
HOMO-7	−8.99	9	2	85	3	−8.97	11	2	44	44
HOMO-6	−8.98	0	0	1	99	−8.96	10	1	44	44
HOMO-5	−8.91	1	0	2	96	−8.79	52	7	21	21
HOMO-4	−8.8	65	11	18	7	−8.74	62	6	16	16
HOMO-3	−8.42	19	3	40	38	−8.65	5	4	45	45
HOMO-2	−8.28	25	3	30	42	−8.28	14	2	42	42
HOMO-1	−8.03	18	2	57	23	−8.14	5	1	47	47
HOMO	**−7.96**	**29**	**2**	**24**	**45**	**−7.84**	**38**	**3**	**30**	**30**
LUMO	**−4.75**	**4**	**93**	**1**	**1**	**−4.64**	**4**	**95**	**1**	**1**
LUMO+1	−3.77	4	93	2	2	−3.67	3	93	2	2
LUMO+2	−3.56	1	98	1	1	−3.44	1	98	1	1
LUMO+3	−3.1	8	5	4	82	−3.12	8	6	43	43
LUMO+4	−2.9	5	2	84	9	−3.07	7	3	45	45
LUMO+5	−2.81	4	3	28	66	−2.86	3	3	47	47
LUMO+6	−2.69	2	3	70	25	−2.73	3	3	47	47
LUMO+7	−2.49	2	1	90	8	−2.49	3	0	48	48
LUMO+8	−2.46	2	2	8	88	−2.44	0	0	50	50

reasons, the two Ir−N_{dmbpy} distances (2.104(6) and 2.041(6) Å) are different because they have a C-donor atom and an N-triazole atom in trans, respectively.

Quantum Chemical Calculations. Figure 4 shows the optimized molecular structure of the isolated **N,N-cis-3** and **N,N-trans-3** isomers. The high symmetry in **N,N-trans-3** does not introduce differences between the two C^N ligands, while for **N,N-cis-3** the two C^N ligands have to be distinguished: C^N2, where the N of the triazole ring linked to the Ir is trans to dmbpy, and C^N1, with the triazole ring trans to the C-atom of C^N2 (Figure 4). In general, the calculated bond lengths and angles compare well with the experimental values determined by X-ray diffraction (see Table S1). The difference in symmetry between isomers can also be observed in the calculated electronic distribution of the HOMO (Figure 4). In **N,N-trans-3**, the orbitals are equally delocalized over the two C^N ligands, while in **N,N-cis-3**, they have a much stronger asymmetric distribution. The contributions of the different fragments to the frontier occupied and virtual orbitals are collected in Table 1.

Both isomers show an important contribution of the Ir in the HOMO orbital. The metal contribution is the highest in the HOMO-4 in both complexes as well as in the HOMO-5 in the **N,N-trans-3** complex. The other contribution from the HOMO to HOMO-9 levels originates from the cyclometalated ligands. Interestingly, the HOMO in **N,N-cis-3** is less localized on C^N1 (24%) than on C^N2 (45%), where there is a dominant contribution from the phenyl ring (32%) and a smaller weight on the triazole part (13%). The first occupied orbitals strongly localized on the diimine ligand are HOMO-11 and HOMO-10 for the **N,N-cis-3** and **N,N-trans-3**, respectively. In both complexes, the LUMO is localized predominantly on the diimine ligand, as has been observed recently for analogous complexes.[25,32] The LUMO+1 and LUMO+2 levels have also a dominant weight on the diimine ligand, whereas the LUMO+3 to LUMO+8 levels have the largest ligand contribution arising from the C^N units.

Photophysical Properties. The absorption spectra of complexes **N,N-trans-3** and **N,N-cis-3** were recorded at room temperature in dichloromethane solution (Figure 5). Compared to that of **N,N-trans-3**, the UV−vis absorption spectrum of **N,N-cis-3** is slightly red-shifted. The intense bands ($\varepsilon > 10^4$ $M^{-1}cm^{-1}$) at high energy (220−310 nm) are assigned to $\pi-\pi^*$ ligand-centered (LC) transition localized on the coordinated ligands (Table 2). Weaker absorption bands at longer wavelengths (310−450 nm) are assigned to spin-allowed and spin-forbidden charge transfer (CT) transitions. In this region, the higher energy bands are described as metal-to-ligand CT (^{1}MLCT) transitions involving the metal orbitals and the π orbitals of the cyclometalated or diimine ligand and ligand-to-ligand CT (LLCT), similarly to analogous energies bands in related phenylpyrazolyl- and aryltriazolyl-based complexes recently described.[25,32] The lower energy absorptions are assigned to the $(C^N)_2$Ir-to-dmbpy ligand transition, ^{3}MLCT. These bands are higher in energy than those of phenylpyridyl analogues.[16,25,52] However, in our complexes the MLCT character seems even more pronounced than for cationic complexes containing phenylpyridyl and bipyridine ligands.[52]

In order to assist the interpretation of the experimental absorption spectra, TD-DFT calculations were performed to examine the nature of the low-lying singlet excited states at the optimized geometry of the ground state. Table 3 shows the singlet transitions from the ground state that mostly contribute to the absorption spectra, while Figure 6 shows the simulated absorption spectra covering the lowest 300 singlet transitions in energy.

Table 3 summarizes the experimental absorption features of the isomers in dichloromethane, DCM, as well as the excited states contributing to the absorption peaks. The theoretical results are in agreement with the experimental results. As expected from related phenylpyrazolyl-based complexes,[25] the absorption peaks at lower energy have a MLCT and/or LLCT

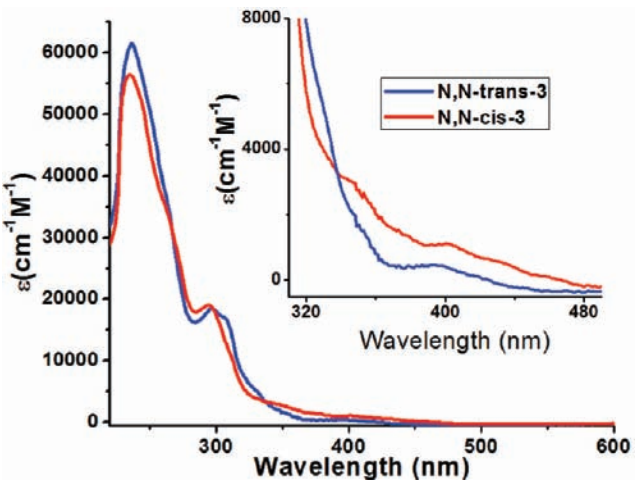

Figure 5. Absorption spectra for **N,N-trans-3** and **N,N-cis-3** in dichloromethane.

Table 3. Comparison of Experimental and Simulated Absorption Spectra Characteristics

exptl (in DCM)		theory		
λ, nm	ε, $\times 10^4$ M^{-1} cm^{-1}	λ, nm	OS[a]	character
		N,N-cis-3		
435	0.05	485	0.004	MLCT, LLCT
401	0.1	462	0.007	LLCT, MLCT
346	0.3	370	0.061	MLCT, LLCT
295	1.9	289	0.052	MLCT, LC
		275	0.072	MLCT, LC
		267	0.189	MLCT, LC
235	5.6	237	0.191	MLCT, LC
		236	0.138	LC, MLCT
		230	0.105	LC, MLCT
		N,N-trans-3		
445	–	485	0	MLCT, LLCT
393	0.05	414	0.008	LLCT
330	0.5	356	0.053	LLCT, MLCT
307	1.7	287	0.067	MLCT, LC
		275	0.126	MLCT, LC
296	1.8	267	0.053	MLCT, LC
		263	0.077	LLCT, LC
		260	0.106	MLCT, LC
237	6.1	243	0.32	LC, MLCT
		242	0.255	MLCT, LC

[a] Oscillator strength directly linked to the molecular extinction coefficient.

Table 2. Photophysical Data for N,N-trans-3 and N,N-cis-3

solvent	abs, λ/nm (ε, $\times 10^4$ M^{-1} cm^{-1})	Em, λ/nm	Φ_{deaer} (Φ_{aer})[b]	τ_{deaer} (τ_{aer}), μs	k_r, 10^5 s^{-1}	k_{nr}, 10^5 s^{-1}
		N,N-trans-3				
DCM	237 (6.1), 296 (1.8), 307 (1.7), 330 (sh, 0.5), 393 (0.05), 445	488	0.85 (0.21)	1.46 (0.29)	5.8	1.0
MeCN		497	0.81 (0.06)	1.44 (0.10)	5.6	1.3
DMSO		498	0.85 (0.22)	1.27 (0.36)	6.7	1.5
butyronitrile glass[a]		446, 480, 506		3.8		
		N,N-cis-3				
DCM	235 (5.6), 295 (1.9), 346 (0.3), 401 (0.1), 434 (0.05), 460 (0.005)	512	0.87 (0.24)	1.90 (0.57)	4.3	0.7
MeCN		512	0.77 (0.07)	1.83 (0.16)	4.2	1.2
DMSO		512	0.84 (0.24)	1.66 (0.45)	5.0	0.9
butyronitrile glass[a]		464, 494, 527		8.22		

[a] At 77 K. [b] Photoluminescence quantum yields were determined with a calibrated integrating sphere system.

dx.doi.org/10.1021/ja201691b |J. Am. Chem. Soc. 2011, 133, 10543–10558

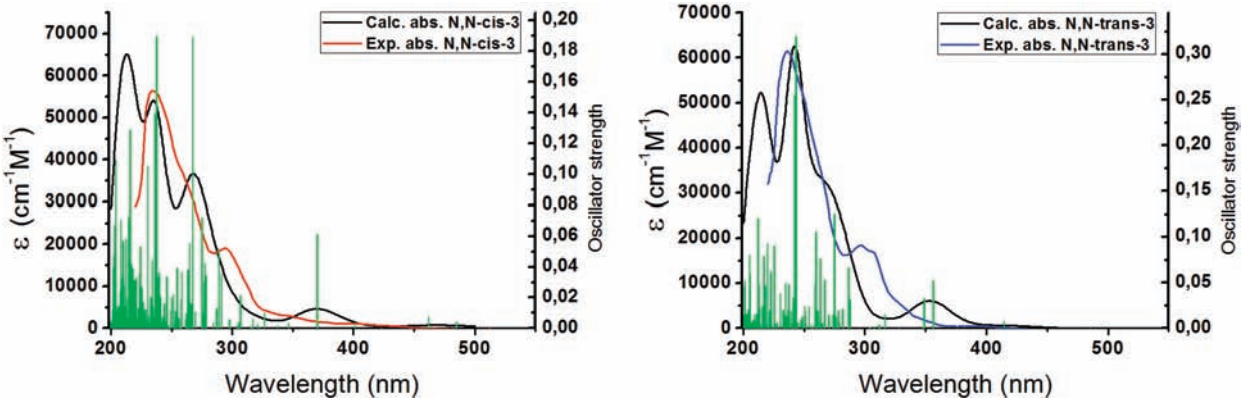

Figure 6. Experimental (red and blue) and simulated (black) absorption spectra of **N,N-cis-3** (left) and **N,N-trans-3** (right), including the oscillator strength of the significant electronic transitions (green bars/right *y* axis) and a broadening of the spectrum with Gaussian functions with a full-width at half-maximum of 3000 cm^{-1} (red line). The intensity of the bands in the convoluted spectrum is expressed with the molecular extinction coefficient (epsilon). The spectrum has been generated with the GaussSum software.[53]

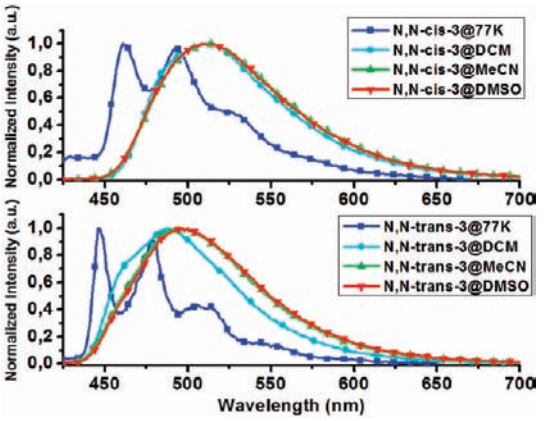

Figure 7. Emission spectra complexes **N,N-cis-3** (top) and **N,N-trans-3** (bottom) in butyronitrile at 77 K (blue) and in dichloromethane (light blue), CH_3CN (green). and DMSO (red) at room temperature.

character, thus rationalizing the weak oscillator. In both cases, the MLCT occurs between the iridium atom and the diimine ligand and the LLCT from the cyclometalated ligands to the diimine ligand. At higher energy, the significant increase in the intensity of the experimental absorption peaks is well reproduced at the theoretical level. This mostly results from the appearance of diimine ligand-centered character in addition to the MLCT transition in the description of the excited states. Note that the two absorption peaks around 300 nm in **N,N-trans-3** are also reproduced in the simulations. The absorption peaks at 235 and 237 nm in **N,N-cis-3** and **N,N-trans-3** have the largest intensity due to the increasing LC contribution at high energy.

Complexes **N,N-trans-3** and **N,N-cis-3** show unstructured emission spectra with maxima at 488 and 512 nm, respectively, in dichloromethane at room temperature (Figure 7). These unstructured spectra are typical of Ir(III) complexes containing a combination of cyclometalated (C^N) and neutral diimine ligands.[16,25,52,54] Interestingly, the emission maximum in **N,N-trans-3** is blue-shifted (ca. 24 nm) compared to those of both **N,N-cis-3** and difluorophenylpyridine (dfppy) analogues $[Ir(dfppy)(N^N)]^+$ (N^N = diimine) described in the literature.[52,55] The emission spectra of both isomers at 77 K in butyronitrile glass matrix show a rigidochromic blue shift (ca. 50 nm) compared to the spectra at room temperature. This behavior together with the unstructured spectra of the complexes at room temperature suggests a pronounced ^{3}MLCT character of the emissive state of these complexes, similarly to the analogous complex *N,N-trans*-$[Ir(C^N)_2(bpy)](PF_6)$ (C^N = 4-phenyl-1*H*-1,2,3-triazolyl) described recently in the literature.[32] Furthermore, complex **N,N-trans-3** exhibits solvatochromic behavior in the emission spectra on going from dichloromethane (λ_{em} = 488 nm) to more polar solvents such as acetonitrile (λ_{em} = 497 nm) or DMSO (λ_{em} = 497 nm), while **N,N-cis-3** shows no changes (Figure 7). On the other hand, the lifetimes for **N,N-cis-3** in different solvents (both deaerated and aerated solutions) are longer than for **N,N-trans-3**, with the most significant difference at 77 K in glass matrix (Table 2). The differences in emission spectra and lifetimes and also the higher radiative constants (k_r) for the **N,N-trans-3** isomer compared to the **N,N-cis-3** suggest a higher MLCT character in the emitting excite state of the former.

The photoluminescence quantum yields (Φ) of **N,N-trans-3** and **N,N-cis-3** in deaerated solutions are very high (over 85%), making these complexes some of the most efficient cationic phosphorescent complexes ever reported. Furthermore, both complexes present remarkably high emission quantum yields (10−22%) in air-equilibrated solution. These values are higher than those reported in the literature, which are typically below 5%.[12]

The TD-DFT calculations show that the lowest triplet excited state in both complexes is mostly described by a HOMO-to-LUMO transition (Table 4). In both cases, the lowest triplet state shows a mixing of ^{3}MLCT and ^{3}LLCT character, which is consistent with the unstructured shape of the emission spectrum. The calculated emission wavelength for **N,N-trans-3** is 488 nm, which matches very well the experimental value in dichloromethane, and is shifted to 498 nm for **N,N-cis-3**, in agreement with the experimental trends. We have further collected in Table 5 the dipole moments in the ground state (S_0) and the lowest singlet (S_1) and triplet (T_1) excited states. The large difference between the calculated dipole moments in the ground state and lowest triplet excited state for **N,N-trans-3** rationalizes its solvatochromic behavior, which is expected to be strongly limited in **N,N-cis-3** due to the similar calculated values. When going to more polar solvents, the lowest triplet state will be more stabilized than the ground state, therefore reducing the energy of the first emission peak, as observed experimentally when going from dichloromethane to acetonitrile or DMSO.

Table 4. Characterization of the Lowest Triplet Excited State at the TD-DFT Level in the Absence of Spin-Orbit Coupling for N,N-cis-3 and N,N-trans-3

complex	Occ	Vir	eV/nm	%	character
N,N-cis-3	HOMO	LUMO	2.49/498	79	C^N1 → NN (22%), C^N2 → NN (42%), Ir → NN (27%)
N,N-trans-3	HOMO	LUMO	2.54/488	98	Ir → NN (36%), C^N1 → NN (29%), C^N2 → NN (29%)

Table 5. Total Dipole Moments of the Ground State (S_0), First Singlet Excited State (S_1), and First Triplet State (T_1) for N,N-cis-3 and N,N-trans-3[a]

N,N-cis-3		N,N-trans-3	
state	dipole, D	state	dipole, D
S_0	5.60	S_0	2.66
S_1	6.22	S_1	2.67
T_1	5.69	T_1	8.28

[a] In both cases, the geometry of the complex corresponds to that of the ground state.

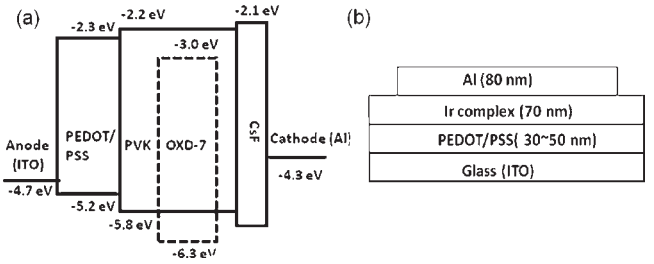

Figure 8. (a) Structure of PLED devices and energy levels of materials used in this study. (b) Structure of LEEC devices.

Electrochemistry. The electrochemical behavior of the complexes **N,N-trans-3** and **N,N-cis-3** was investigated by cyclic voltammetry (CV) and differential pulse voltammetry (DPV) in a 0.1 M solution of TBAH in acetonitrile. The complexes show a reversible electrochemical behavior in both positive and negative bias. Complex **N,N-trans-3** shows a first oxidation wave at +1.66 V and a reduction wave at −1.41 V, while **N,N-cis-3** shows a slightly higher oxidation +1.70 V and a reduction wave at −1.31 V (Figures S14 and S15). The electrochemical band gap has been estimated as the difference between the standard potentials ($E°$) of the first redox processes occurring in the negative (reduction) and positive (oxidation) biases, respectively ($\Delta E° = E°_{ox} - E°_{red}$), and it is slightly higher for **N,N-trans-3** (3.07 V) than for **N,N-cis-3** (3.01 V). The DFT calculations yield similar band gaps (HOMO−LUMO) of 3.21 and 3.20 eV, respectively. As reported in the literature for complexes of the type $[Ir(C^N)_2(N^N)]^+$ (C^N = ppy, dfppy, or ppz; N^N = bipyridyl ligand),[25] we expect that the oxidation is associated with the bis-cyclometalated phenyl-Ir moiety, while the reduction occurs on the bipyridyl ligand, as supported by the localization of the HOMO and LUMO orbitals given by DFT calculations. **N,N-trans-3** shows a lower oxidation potential and a higher reduction potential than **N,N-cis-3**; a similar trend is observed at the theoretical level.

Electroluminescent Devices. Recently, charged Ir(III) complexes have been employed in solution-processed PLEDs and LEECs.[9,56,57] Until now, no literature reported the comparison of the electroluminescent device behavior between two charged bis-cyclometalated Ir(III) geometrical isomers. Therefore, we decided to prepare the PLED and even the LEEC devices using the isomers **N,N-cis-3** and **N,N-trans-3** as emitting compounds.

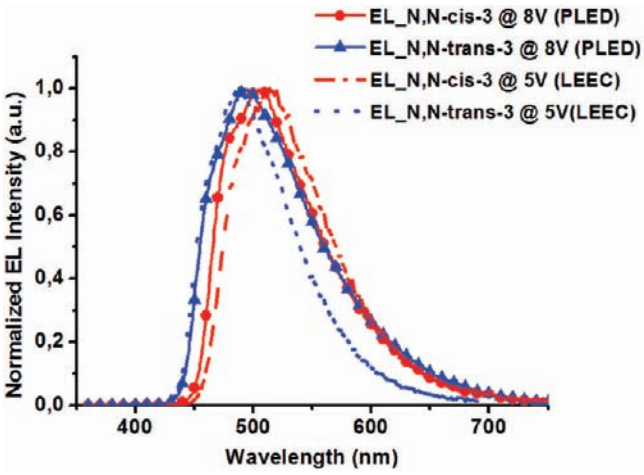

Figure 9. Compared EL spectra form PLED (at 8 V) and LEEC (at 5 V) devices for the complexes **N,N-cis-3** and **N,N-trans-3**.

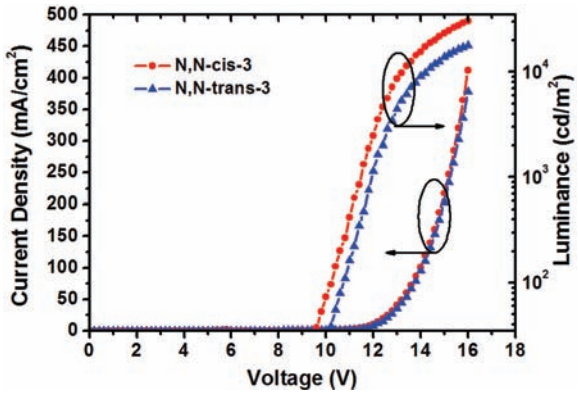

Figure 10. Current density−voltage−luminance (*IVL*) characteristics of devices of **N,N-cis-3** and **N,N-trans-3**.

Solution-processed PLEDs with **N,N-cis-3** or **N,N-trans-3** were fabricated under inert conditions, using the studied compounds as dopants in a poly(9-vinylcarbazole) (PVK) matrix. PVK is known to be a preferentially hole-transporting material. Therefore, we blended the PVK with an electron-transporting material, 2,2′-(1,3-phenylene)bis[5-[4-(1,1-dimethylethyl)-phenyl]]-1,3,4-oxadiazole (OXD-7) to enable the host to transport both electrons and holes. Poly(3,4-ethylenedioxythiophene): polystyrene sulfonate (PEDOT:PSS) as a hole-injecting layer

Table 6. Summary of Device Characteristics for PLEDs

device (10 wt % dopant)	V_{on},[a,d] V	L_{max},[b] cd/m^2	$\eta_{ext,max}$,[c,d] %	$\eta_{c,max}$,[d] cd/A	CIE (x, y)[e]
N,N-cis-3	7.4	30 466 (16 V)	8.8	25.8	(0.27, 0.49)
N,N-trans-3	7.6	18 017(16 V)	5.2	14.2	(0.26, 0.43)

[a] Turn-on voltage recorded at 1 cd/m^2. [b] Maximum luminance. [c] Maximum external quantum efficiency. [d] Maximum current efficiency. [e] Commission International de l'Eclairage coordinates at 8 V.

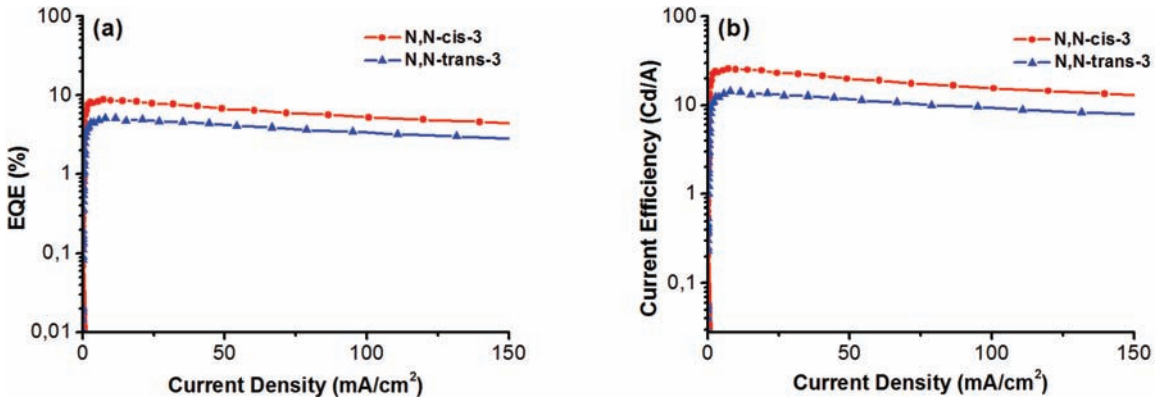

Figure 11. (a) External quantum efficiency (EQE) devices. (b) Current efficiency of devices.

and 1,3,5-tris[*N*-(phenyl)benzimidazole]benzene (TPBI) as an electron-transporting/hole-blocking layer were employed. The solution-processed device structure can be represented as follows: glass/ITO/PEDOT:PSS (50 nm)/PVK:OXD-7 (7:3) + Ir emitter (10 wt %) (100 nm)/TPBI (30 nm)/CsF (1.5 nm)/Al (80 nm) (see Experimental Section for more details). The doping concentration for the iridium emitters was 10% by weight. In Figure 8 are shown the structures of the PLED and LEEC devices and the energy levels of the compounds used in this study.

Figure 9 shows the electroluminescence (EL) spectra of complexes **N,N-cis-3** and **N,N-trans-3** for the studied devices at 8 V. No emission coming from the host polymer matrix was observed, meaning that efficient energy transfer from the host to the guest iridium complexes occurs. The PVK:OXD-7-based PLEDs using **N,N-cis-3** and **N,N-trans-3** as the emitters show EL spectra with a maximum at 508 and 497 nm, respectively. The EL spectra of both complexes are almost identical to the photoluminescence (PL) spectra in solution. Both devices show bright blue-green light emission, and the Commission International de l'Eclairage (CIE) coordinates of the emitted light are x = 0.27 and y = 0.49 for **N,N-cis-3** and x = 0.26 and y = 0.43 for **N,N-trans-3.** The plot of luminance vs voltage for the devices is shown in Figure 10. The turn-on voltage (V_{on}), i.e., the voltage needed to reach 1 cd/m^2, is about 7.4 V (**N,N-cis-3**) and 7.6 V (**N,N-trans-3**) (Table 6). The maximum luminance for the **N,N-cis-3** (30 466 cd/m^2) is higher than for **N,N-trans-3** (18 017 cd/m^2) at 16 V. From Figure 11, we can observe that the EQE and current efficiency (cd/A) of **N,N-cis-3** also show superior performance. The maximum EQE and current efficiency of the **N,N-cis-3** device are around 8.8% and 25.8 cd/A (at 7.2 mA/cm^2), while for the **N,N-trans-3** device, the values are 5.2% and 14.2 cd/A (at 8.2 mA/cm^2). Based on the above device data, the **N,N-cis-3** complex exhibits a better performance in PLEDs than the **N,N-trans-3**. Furthermore, these high-efficiency device values are comparable with those of green-emitting charged iridium complexes.[56]

Table 7. Summary of Device Characteristics for LEEC

device	voltage, V	t_{max},[a] s	L_{max},[b] cd/m^2	CIE (x, y)[c]
N,N-cis-3	5.0	180	115	(0.29, 0.51)
N,N-trans-3	5.0	360	62	(0.26, 0.41)

[a] Time required to reach the maximum luminance. [b] Maximum luminance value for a constant voltage of 5.0 V applied to the device. [c] Commission International de l'Eclairage coordinates under a constant bias voltage 5.0 V.

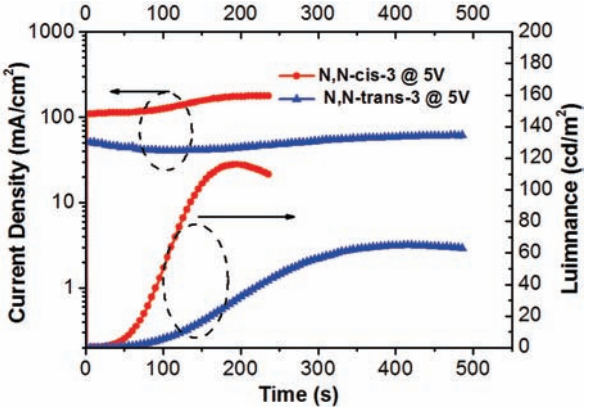

Figure 12. Current density and luminance versus time for LEEC.

The LEEC devices were prepared according to the architecture characteristics summarized in Figure 8b. Glass plates on which ITO was sputtered were used as the substrates. Upon applying a bias of 5 V to an ITO/PEDOT:PSS/**N,N-cis-3** or **N,N-trans-3**/Al device, light emission, slowly increasing in intensity with time, reached a maximum luminance at 180 or 360 s, respectively (Table 7). The EL spectra of the two isomers **N,N-cis-3** and **N,N-trans-3** are almost identical with respect to the EL

spectrum obtained from the PLED device and PL spectra in solution (Figure 9). Figure 12 shows the plot of current density and luminance versus time upon applying a continuous bias of 5 V. A rapid increase in the luminance is observed for both **N,N-cis-3** and **N,N-trans-3** devices, reaching luminance of 115 and 62 cd/m^2, respectively. As observed for the PLED devices, the LEEC device of **N,N-cis-3** shows higher luminance than the **N,N-trans-3** device.

CONCLUSIONS

In summary, the synthesis and both photophysical and electrochemical characterization of new Ir(III) complexes utilizing 1,4-disubstituted-1*H*-1,2,3-triazoles as cyclometalating ligands are reported. Depending on the reaction conditions, we can control the mutual arrangement of the heterocyclic rings of the cyclometalated ligands on the Ir(III) dimers. At low temperature, the dimer with a unique *cis*-C,C and *cis*-N,N disposition of the cyclometalated ligands around iridium atom is obtained, while at a higher temperature, the isomer with *cis*-C, C and *trans*-N,N cyclometalated ligands is isolated. Such geometric control of the precursors opens an interesting route to cationic bis-cyclometalated Ir(III) complexes with a *trans*-N,N or *cis*-N,N disposition of the N-heterocyclic rings of the C^N ligands. The two geometrical isomers, **N,N-trans-3** and **N,N-cis-3**, show different photophysical properties depending on the mutual orientation of the cyclometalated ligands. DFT calculations point to symmetry effects as the principal reason for the differences in emission between the isomeric forms. The different arrangement of the cyclometalated ligands in cationic Ir(III) complexes also has an implication on the application of these complexes, as shown by their different behavior in electroluminescent devices, where **N,N-cis-3** isomer presents a higher luminance than **N,N-trans-3**, both in PLED and LEEC. Due to the wide use of luminescent cationic bis-cyclometalated Ir(III) complexes in several fields and the fact that *cis*-N,N isomers have not been reported, the results presented herein open a door for further studies on these kind of isomers and their optoelectronic applications.

ASSOCIATED CONTENT

Supporting Information. X-ray crystallographic data files (CIF), crystal data, structure refinement parameters, and NMR spectra for **N,N-cis-dimer**, **N,N-cis-2b**, **N,N-trans-2b**, **N,N-trans-3′**, and **N,N-cis-3**; HPLC chromatograms, cyclic voltammograms, and comparison of theoretical and experimental representative distances and bond angles for **N,N-trans-3** and **N,N-cis-3**. This material is available free of charge via the Internet at http://pubs.acs.org.

AUTHOR INFORMATION

Corresponding Author

jfern_01@uni-muenster.de; decola@uni-muenster.de

ACKNOWLEDGMENT

J.M.F.-H. acknowledges Fundación Séneca (Agencia Regional de Investigación, Región de Murcia) for funding and Drs. María Dolores Gálvez-López and Leonard L. Tinker for fruitful discussions. C.-H.Y. thanks the Humboldt Foundation for financial support. The work in Mons is supported by the Belgian National Fund for Scientific Research (FNRS). This research used resources of the Interuniversity Scientific Computing Facility located at the University of Namur, Belgium, which is supported by the F.R.S.-FNRS under convention No. 2.4617.07. J.C. is a senior research associate of FNRS.

REFERENCES

(1) Lo, K. K. W.; Chung, C. K.; Lee, T. K. M.; Lui, L. H.; Tsang, K. H. K.; Zhu, N. Y. *Inorg. Chem.* **2003**, *42*, 6886–6897. Lo, K. K. W.; Hui, W. K.; Chung, C. K.; Tsang, K. H. K.; Lee, T. K. M.; Li, C. K.; Lau, J. S. Y.; Ng, D. C. M. *Coord. Chem. Rev.* **2006**, *250*, 1724–1736. Yu, M. X.; Zhao, Q.; Shi, L. X.; Li, F. Y.; Zhou, Z. G.; Yang, H.; Yia, T.; Huang, C. H. *Chem. Commun.* **2008**, 2115–2117. Zhao, Q.; Yu, M. X.; Shi, L. X.; Liu, S. J.; Li, C. Y.; Shi, M.; Zhou, Z. G.; Huang, C. H.; Li, F. Y. *Organometallics* **2010**, *29*, 1085–1091.

(2) Metz, S.; Bernhard, S. *Chem. Commun.* **2010**, *46*, 7551–7553. Curtin, P. N.; Tinker, L. L.; Burgess, C. M.; Cline, E. D.; Bernhard, S. *Inorg. Chem.* **2009**, *48*, 10498–10506. Tinker, L. L.; Bernhard, S. *Inorg. Chem.* **2009**, *48*, 10507–10511. Tinker, L. L.; McDaniel, N. D.; Bernhard, S. *J. Mater. Chem.* **2009**, *19*, 3328–3337. Cline, E. D.; Adamson, S. E.; Bernhard, S. *Inorg. Chem.* **2008**, *47*, 10378–10388. Lowry, M. S.; Goldsmith, J. I.; Slinker, J. D.; Rohl, R.; Pascal, R. A.; Malliaras, G. G.; Bernhard, S. *Chem. Mater.* **2005**, *17*, 5712–5719. Goldsmith, J. I.; Hudson, W. R.; Lowry, M. S.; Anderson, T. H.; Bernhard, S. *J. Am. Chem. Soc.* **2005**, *127*, 7502–7510. King, K. A.; Spellane, P. J.; Watts, R. J. *J. Am. Chem. Soc.* **1985**, *107*, 1431–1432.

(3) DeRosa, M. C.; Hodgson, D. J.; Enright, G. D.; Dawson, B.; Evans, C. E. B.; Crutchley, R. J. *J. Am. Chem. Soc.* **2004**, *126*, 7619–7626. Gao, R. M.; Ho, D. G.; Hernandez, B.; Selke, M.; Murphy, D.; Djurovich, P. I.; Thompson, M. E. *J. Am. Chem. Soc.* **2002**, *124*, 14828–14829.

(4) Zhao, Q.; Li, F. Y.; Liu, S. J.; Yu, M. X.; Liu, Z. Q.; Yi, T.; Huang, C. H. *Inorg. Chem.* **2008**, *47*, 9256–9264. Zhao, Q.; Li, F.; Huang, C. H. *Chem. Soc. Rev.* **2010**, *39*, 3007–3030.

(5) Yersin, H. *Highly Efficient OLEDs with Phosphorescent Materials*; Wiley-VCH: Weinheim, 2008. Adachi, C.; Baldo, M. A.; Thompson, M. E.; Forrest, S. R. *J. Appl. Phys.* **2001**, *90*, 5048–5051. Baldo, M. A.; O'Brien, D. F.; You, Y.; Shoustikov, A.; Sibley, S.; Thompson, M. E.; Forrest, S. R. *Nature* **1998**, *395*, 151–154.

(6) Orselli, E.; Kottas, G. S.; Konradsson, A. E.; Coppo, P.; Frohlich, R.; Frtshlich, R.; De Cola, L.; van Dijken, A.; Buchel, M.; Borner, H. *Inorg. Chem.* **2007**, *46*, 11082–11093.

(7) Thompson, M. E.; Djurovich, P. E.; Barlow, S.; Marder, S. In *Comprehensive Organometallic Chemistry III*; Elsevier: Oxford, 2007; Vol. 12, pp 101−194.

(8) Mydlak, M.; Bizzarri, C.; Hartmann, D.; Sarfert, W.; Schmid, G.; De Cola, L. *Adv. Funct. Mater.* **2010**, *20*, 1812–1820.

(9) Yang, C. H.; Beltran, J.; Lemaur, V.; Cornil, J.; Hartmann, D.; Sarfert, W.; Frohlich, R.; Bizzarri, C.; De Cola, L. *Inorg. Chem.* **2010**, *49*, 9891–9901.

(10) Di Censo, D.; Fantacci, S.; De Angelis, F.; Klein, C.; Evans, N.; Kalyanasundaram, K.; Bolink, H. J.; Gratzel, M.; Nazeeruddin, M. K. *Inorg. Chem.* **2008**, *47*, 980–989. Nazeeruddin, M. K.; Wegh, R. T.; Zhou, Z.; Klein, C.; Wang, Q.; De Angelis, F.; Fantacci, S.; Gratzel, M. *Inorg. Chem.* **2006**, *45*, 9245–9250. Parker, S. T.; Slinker, J. D.; Lowry, M. S.; Cox, M. P.; Bernhard, S.; Malliaras, G. G. *Chem. Mater.* **2005**, *17*, 3187–3190.

(11) Lowry, M. S.; Bernhard, S. *Chem.—Eur. J.* **2006**, *12*, 7970–7977.

(12) Flamigni, L.; Barbieri, A.; Sabatini, C.; Ventura, B.; Barigelletti, F. *Top. Curr. Chem.* **2007**, *281*, 143–203.

(13) Nonoyama, M. *Bull. Chem. Soc. Jpn.* **1974**, *47*, 767–768.

(14) Garces, F. O.; King, K. A.; Watts, R. J. *Inorg. Chem.* **1988**, *27*, 3464–3471. Garces, F. O.; Dedeian, K.; Keder, N. L.; Watts, R. J. *Acta Crystallogr. C* **1993**, *49*, 1117–1120. Lamansky, S.; Djurovich, P.; Murphy, D.; Abdel-Razzaq, F.; Kwong, R.; Tsyba, I.; Bortz, M.; Mui, B.; Bau, R.; Thompson, M. E. *Inorg. Chem.* **2001**, *40*, 1704–1711. Graf, M.; Thesen, M.; Krüger, H.; Mayer, P.; Sünkel, K. *Inorg. Chem. Commun.*

2009, *12*, 701–703. Bettington, S.; Thompson, A. L.; Beeby, A.; Goeta, A. E. *Acta Crystallogr. E* **2004**, *60*, m827–m829. Krisyuk, V.; Turgambaeva, A.; Lee, J.; Rhee, S.-W. *Trans. Met. Chem.* **2005**, *30*, 786–791.

(15) Ulbricht, C.; Beyer, B.; Friebe, C.; Winter, A.; Schubert, U. S. *Adv. Mater.* **2009**, *21*, 4418–4441.

(16) Tamayo, A. B.; Alleyne, B. D.; Djurovich, P. I.; Lamansky, S.; Tsyba, I.; Ho, N. N.; Bau, R.; Thompson, M. E. *J. Am. Chem. Soc.* **2003**, *125*, 7377–7387.

(17) Karatsu, T.; Nakamura, T.; Yagai, S.; Kitamura, A.; Yamaguchi, K.; Matsushima, Y.; Iwata, T.; Hori, Y.; Hagiwara, T. *Chem. Lett.* **2003**, *32*, 886–887. Karatsu, T.; Ito, E.; Yagai, S.; Kitamura, A. *Chem. Phys. Lett.* **2006**, *424*, 353–357. McDonald, A. R.; Lutz, M.; von Chrzanowski, L. S.; van Klink, G. P. M.; Spek, A. L.; van Koten, G. *Inorg. Chem.* **2008**, *47*, 6681–6691. Tsuchiya, K.; Ito, E.; Yagai, S.; Kitamura, A.; Karatsu, T. *Eur. J. Inorg. Chem.* **2009**, 2104–2109. Deaton, J. C.; Young, R. H.; Lenhard, J. R.; Rajeswaran, M.; Huo, S. Q. *Inorg. Chem.* **2010**, *49*, 9151–9161.

(18) Dedeian, K.; Shi, J. M.; Shepherd, N.; Forsythe, E.; Morton, D. C. *Inorg. Chem.* **2005**, *44*, 4445–4447.

(19) Holmes, R. J.; Forrest, S. R.; Sajoto, T.; Tamayo, A.; Djurovich, P. I.; Thompson, M. E.; Brooks, J.; Tung, Y. J.; D'Andrade, B. W.; Weaver, M. S.; Kwong, R. C.; Brown, J. J. *Appl. Phys. Lett.* **2005**, *87*, 243507. Ren, X. F.; Kondakova, M. E.; Giesen, D. J.; Rajeswaran, M.; Madaras, M.; Lenhart, W. C. *Inorg. Chem.* **2010**, *49*, 1301–1303.

(20) Lamansky, S.; Djurovich, P.; Murphy, D.; Abdel-Razzaq, F.; Lee, H. E.; Adachi, C.; Burrows, P. E.; Forrest, S. R.; Thompson, M. E. *J. Am. Chem. Soc.* **2001**, *123*, 4304–4312. Li, J.; Djurovich, P. I.; Alleyne, B. D.; Yousufuddin, M.; Ho, N. N.; Thomas, J. C.; Peters, J. C.; Bau, R.; Thompson, M. E. *Inorg. Chem.* **2005**, *44*, 1713–1727. You, Y.; Kim, K. S.; Ahn, T. K.; Kim, D.; Park, S. Y. *J. Phys. Chem. C* **2007**, *111*, 4052–4060. Chou, P.-T.; Chi, Y. *Chem.—Eur. J.* **2007**, *13*, 380–395. Chi, Y.; Chou, P. T. *Chem. Soc. Rev.* **2010**, *39*, 638–655.

(21) You, Y. M.; Park, S. Y. *J. Am. Chem. Soc.* **2005**, *127*, 12438–12439.

(22) Baranoff, E.; Suarez, S.; Bugnon, P.; Barolo, C.; Buscaino, R.; Scopelliti, R.; Zuppiroli, L.; Graetzel, M.; Nazeeruddin, M. K. *Inorg. Chem.* **2008**, *47*, 6575–6577. Baranoff, E.; Bolink, H. J.; De Angelis, F.; Fantacci, S.; Di Censo, D.; Djellab, K.; Gratzel, M.; Nazeeruddin, M. K. *Dalton Trans.* **2010**, *39*, 8914–8918.

(23) Hung, J.-Y.; Chi, Y.; Pai, I. H.; Yu, Y.-C.; Lee, G.-H.; Chou, P.-T.; Wong, K.-T.; Chen, C.-C.; Wu, C.-C. *Dalton Trans.* **2009**, 6472–6475.

(24) You, Y.; Park, S. Y. *Dalton Trans.* **2009**, 1267–1282.

(25) Tamayo, A. B.; Garon, S.; Sajoto, T.; Djurovich, P. I.; Tsyba, I. M.; Bau, R.; Thompson, M. E. *Inorg. Chem.* **2005**, *44*, 8723–8732.

(26) Sajoto, T.; Djurovich, P. I.; Tamayo, A. B.; Oxgaard, J.; Goddard, W. A.; Thompson, M. E. *J. Am. Chem. Soc.* **2009**, *131*, 9813–9822.

(27) Sajoto, T.; Djurovich, P. I.; Tamayo, A.; Yousufuddin, M.; Bau, R.; Thompson, M. E.; Holmes, R. J.; Forrest, S. R. *Inorg. Chem.* **2005**, *44*, 7992–8003.

(28) Orselli, E.; Albuquerque, R. Q.; Fransen, P. M.; Frohlich, R.; Janssen, H. M.; De Cola, L. *J. Mater. Chem.* **2008**, *18*, 4579–4590. Felici, M.; Contreras-Carballada, P.; Vida, Y.; Smits, J. M. M.; Nolte, R. J. M.; De Cola, L.; Williams, R. M.; Feiters, M. C. *Chem.—Eur. J.* **2009**, *15*, 13124–13134.

(29) Felici, M.; Contreras-Carballada, P.; Smits, J. M. M.; Nolte, R. J. M.; Williams, R. M.; De Cola, L.; Feiters, M. C. *Molecules* **2010**, *15*, 2039–2059.

(30) Coppo, P.; Plummer, E. A.; De Cola, L. *Chem. Commun.* **2004**, 1774–1775.

(31) Kolb, H. C.; Finn, M. G.; Sharpless, K. B. *Angew. Chem., Int. Ed.* **2001**, *40*, 2004–2021. Bock, V. D.; Hiemstra, H.; van Maarseveen, J. H. *Eur. J. Org. Chem.* **2006**, 51–68. Moses, J. E.; Moorhouse, A. D. *Chem. Soc. Rev.* **2007**, *36*, 1249–1262. Meldal, M.; Tornoe, C. W. *Chem. Rev.* **2008**, *108*, 2952–3015.

(32) Beyer, B.; Ulbricht, C.; Escudero, D.; Friebe, C.; Winter, A.; Gonzalez, L.; Schubert, U. S. *Organometallics* **2009**, *28*, 5478–5488.

(33) Botelho, M. B. S.; Fernandez-Hernandez, J. M.; de Queiroz, T. B.; Eckert, H.; De Cola, L.; de Camargo, A. S. S. *J. Mater. Chem.* **2011**, DOI: 10.1039/C1JM10878F.

(34) Otwinowski, Z.; Borek, D.; Majewski, W.; Minor, W. *Acta Crystallogr. A* **2003**, *59*, 228–234.

(35) Blessing, R. H. *J. Appl. Crystallogr.* **1997**, *30*, 421–426. Weeks, C. M.; Hauptman, H. A.; Smith, G. D.; Blessing, R. H.; Teeter, M. M.; Miller, R. *Acta Crystallogr. D* **1995**, *51*, 33–38.

(36) Sheldrick, G. M. *Acta Crystallogr. A* **1990**, *46*, 467–473.

(37) Sheldrick, G. M. *Acta Crystallogr. A* **2008**, *64*, 112–122.

(38) SCHAKAL-97, A computer program for the graphic representation of molecular and crystallographic models. Egbert Keller, Universität Freiburg, 1997.

(39) Lee, C. T.; Yang, W. T.; Parr, R. G. *Phys. Rev. B* **1988**, *37*, 785–789. Becke, A. D. *J. Chem. Phys.* **1993**, *98*, 5648–5652.

(40) Curtiss, L. A.; Redfern, P. C.; Raghavachari, K.; Pople, J. A. *J. Chem. Phys.* **2001**, *114*, 108–117.

(41) Chiodo, S.; Russo, N.; Sicilia, E. *J. Chem. Phys.* **2006**, 125.

(42) Avilov, I.; Minoofar, P.; Cornil, J.; De Cola, L. *J. Am. Chem. Soc.* **2007**, *129*, 8247–8258.

(43) Vlcek, A.; Zalis, S. *Coord. Chem. Rev.* **2007**, *251*, 258–287.

(44) Wang, Z.-X.; Zhao, Z.-G. *J. Heterocycl. Chem.* **2007**, *44*, 89–92. Sreedhar, B.; Reddy, P. S. *Synth. Commun.* **2007**, *37*, 805–812. Appukkuttan, P.; Dehaen, W.; Fokin, V. V.; Van der Eycken, E. *Org. Lett.* **2004**, *6*, 4223–4225.

(45) Sprouse, S.; King, K. A.; Spellane, P. J.; Watts, R. J. *J. Am. Chem. Soc.* **1984**, *106*, 6647–6653. Schmid, B.; Garces, F. O.; Watts, R. J. *Inorg. Chem.* **1994**, *33*, 9–14.

(46) McGee, K. A.; Mann, K. R. *Inorg. Chem.* **2007**, *46*, 7800–7809.

(47) See, for example: Pinillos, M. T.; Elduque, A.; Oro, L. A. *J. Organomet. Chem.* **1988**, *338*, 411–419. Ma, B.; Li, J.; Djurovich, P. I.; Yousufuddin, M.; Bau, R.; Thompson, M. E. *J. Am. Chem. Soc.* **2004**, *127*, 28–29. Urankar, D.; Pinter, B.; Pevec, A.; De Proft, F.; Turel, I.; Kosmrlj, J. *Inorg. Chem.* **2010**, *49*, 4820–4829. Aromí, G.; Barrios, L. A.; Roubeau, O.; Gamez, P. *Coord. Chem. Rev.* **2011**, *255*, 485–546.

(48) Tejel, C.; Ciriano, M. A.; Edwards, A. J.; Lahoz, F. J.; Oro, L. A. *Organometallics* **1997**, *16*, 45–53. Faure, M.; Onidi, A.; Neels, A.; Stoeckli-Evans, H.; Süss-Fink, G. *J. Organomet. Chem.* **2001**, *634*, 12–18. Tejel, C.; Ciriano, M. A.; Millaruelo, M.; Lopez, J. A.; Lahoz, F. J.; Oro, L. A. *Inorg. Chem.* **2003**, *42*, 4750–4758.

(49) Zheng, Y.; Batsanov, A. S.; Bryce, M. R. *Inorg. Chem.* **2011**, *50*, 3354–3362.

(50) Lo, K. K.-W.; Chung, C.-K.; Lee, T. K.-M.; Lui, L.-H.; Tsang, K. H.-K.; Zhu, N. *Inorg. Chem.* **2003**, *42*, 6886–6897. Lo, K. K.-W.; Chan, J. S.-W.; Chung, C.-K.; Tsang, V. W.-H.; Zhu, N. *Inorg. Chim. Acta* **2004**, *357*, 3109–3118. Su, H.-C.; Chen, H.-F.; Fang, F.-C.; Liu, C.-C.; Wu, C.-C.; Wong, K.-T.; Liu, Y.-H.; Peng, S.-M. *J. Am. Chem. Soc.* **2008**, *130*, 3413–3419.

(51) Hazell, A. C.; Hazell, R. G. *Acta Crystallogr.* **1984**, *C40*, 806–811.

(52) Bolink, H. J.; Coronado, E.; Costa, R. D.; Lardiés, N.; Ortí, E. *Inorg. Chem.* **2008**, *47*, 9149–9151.

(53) O'Boyle, N. M.; Tenderholt, A. L.; Langner, K. M. *J. Comput. Chem.* **2008**, *29*, 839–845.

(54) Bolink, H. J.; Cappelli, L.; Cheylan, S.; Coronado, E.; Costa, R. D.; Lardiés, N.; Nazeeruddin, M. K.; Ortí, E. *J. Mater. Chem.* **2007**, 5032–5041.

(55) Lowry, M. S.; Hudson, W. R.; Pascal, R. A.; Bernhard, S. *J. Am. Chem. Soc.* **2004**, *126*, 14129–14135.

(56) Plummer, E. A.; van Dijken, A.; Hofstraat, H. W.; De Cola, L.; Brunner, K. *Adv. Funct. Mater.* **2005**, *15*, 281–289. He, L.; Duan, L.; Qiao, J.; Zhang, D.; Dong, G.; Wang, L.; Qiu, Y. *Org. Electron.* **2009**, *10*, 152–157. He, L.; Duan, L.; Qiao, J.; Zhang, D.; Wang, L.; Qiu, Y. *Org. Electron.* **2010**, *11*, 1185–1191.

(57) Bolink, H. J.; Coronado, E.; Costa, R. D.; Orti, E.; Sessolo, M.; Graber, S.; Doyle, K.; Neuburger, M.; Housecroft, C. E.; Constable, E. C.

Adv. Mater. **2008**, *20*, 3910–3913. Costa, R. D.; Orti, E.; Bolink, H. J.; Graber, S.; Schaffner, S.; Neuburger, M.; Housecroft, C. E.; Constable, E. C. *Adv. Funct. Mater.* **2009**, *19*, 3456–3463. Costa, R. D.; Orti, E.; Bolink, H. J.; Graber, S.; Housecroft, C. E.; Constable, E. C. *J. Am. Chem. Soc.* **2010**, *132*, 5978–5980. Costa, R. D.; Orti, E.; Bolink, H. J.; Graber, S.; Housecroft, C. E.; Constable, E. C. *Adv. Funct. Mater.* **2010**, *20*, 1511–1520.